

May 22, 2019

Electroweak High-Energy Scattering and the Chiral Anomaly

Alan. R. White*

Argonne National Laboratory
9700 South Cass, IL 60439, USA.

Abstract

The effect of perturbative QCD interactions on the high energy scattering of electroweak vector bosons, when the exchanged channel has pion quantum numbers, is considered. It is shown that transverse momentum diagrams appear that have couplings in which the chiral anomaly appears. As a consequence, there is a large transverse momentum divergence that produces an enhancement of the scattering amplitude by a power of the energy. If there is no cancellation from outside of the transverse momentum diagram framework, then the enhancement is present at $O(\alpha_s)$ and involves a single large transverse momentum gluon. In higher orders, soft gluons can accompany the large transverse momentum anomaly process and cancellation of the resulting infra-red divergences is discussed. Odd (anomalous) color parity two gluon exchange, with one gluon carrying finite transverse momentum, also appears at $O(\alpha_s^2)$. Color zero anomalous color parity multigluon exchange first appears at $O(\alpha_s^3)$.

The manipulation of a transverse momentum cut-off to replace the ultra-violet anomaly divergence by infra-red divergences that can lead to confinement and chiral symmetry breaking, is briefly discussed. Possible implications for electroweak symmetry breaking are also noted.

*arw@hep.anl.gov

1. INTRODUCTION

The cancelation of the chiral anomaly in the electroweak sector of the Standard Model is crucial for the existence of the model as a well-defined short-distance field theory. In perturbation theory, the anomaly is a large momentum contribution in axial vector triangle diagrams that, if uncanceled, destroys the renormalizability of a left-handed gauge theory such as the electroweak sector of the Standard Model. In the regge limit the feynman diagrams of standard perturbation theory contract to form transverse momentum diagrams and produce a new perturbation expansion that can be organized into reggeon diagrams[1]-[7]. Beyond leading-log order, the external couplings of the transverse momentum diagrams (which are also the couplings of the reggeon diagrams) contain contracted loop diagrams involving “effective vertices” that result from the contraction. The effective vertices can then produce new “anomalies”, not present in the normal perturbation expansion. For QCD, this is demonstrated in the next-to-leading log calculation[4] of gluon scattering, in which an infra-red (gluon) triangle anomaly is responsible for the helicity non-conservation that occurs, and in our work on the contribution of infra-red quark loop anomalies to pion/pomeron[8] and triple pomeron[9] vertices.

In the electroweak scattering problem considered in this paper, the underlying left-handed theory contains elementary axial vector vertices. It is natural, therefore, that (components of) these elementary vertices will appear also in the regge limit effective vertices. A priori, therefore, large momentum contributions, directly analagous to the familiar triangle anomaly, can be expected within the loop diagrams that contribute to (beyond-leading-order) transverse momentum diagram couplings. Indeed, as we shall see, internal effective vertices, resulting from longitudinal vector meson exchange, also appear which are quark current components that have point interactions only at infinite momentum. Such current components do not appear in the original lagrangian and do not couple to leptons. Consequently, in the electroweak regge limit, we can anticipate a significantly expanded “anomaly problem” which the well-known short distance cancelations, between quarks and leptons, will not be sufficient to remove.

In this paper we will show that the triangle anomaly does indeed appear in the couplings of transverse momentum diagrams that describe the high-energy scattering of $W^{\pm,0}$ vector mesons. All the diagrams we consider describe the exchange of a quark-antiquark pair, with the flavor quantum numbers of the pion, together with some number of gluons. We choose pion quantum numbers because our ultimate goal is to understand the relationship between the anomaly and chiral symmetry breaking in the context of high-energy scattering. Since two fermion exchange is involved, we would expect the energy dependence to be, at most, logarithmic. (Pion

exchange would have no energy dependence.) The signal of the anomaly will be a power divergence of transverse momentum integrals that produces an additional power of the energy in the full amplitude.

Since the anomaly phenomenon we discuss involves longitudinal vector meson states it is natural to expect that the underlying gauge invariance of the electroweak theory will be responsible for some form of cancelation. We discuss this possibility at some length in an Appendix at the end of the paper. While it appears that the anomaly is not completely eliminated, these identities do produce cancelations that can not be straightforwardly expressed in terms of transverse momentum diagram divergences. Moreover, it is clear that the large transverse momentum region producing the anomaly could also contribute in an important way within superficially non-leading feynman diagrams. If there is finally a cancelation, then it most likely means the failure of the transverse momentum diagram formalism for the electroweak theory unless (as, in any case, we strongly advocate) a transverse momentum cut-off is imposed from the outset. In the main body of the paper our purpose will be to study contributions to transverse momentum diagrams and, apart from the discussion in Appendix D, and the related discussion in sub-section 3.13, we will make only brief references to the possibility that there could be important contributions outside of the transverse momentum diagram formalism.

The anomaly occurs only in the even signature amplitude, which is a sum of scattering amplitudes for vector mesons with opposite and same sign helicities, i.e.

$$\begin{aligned} A^+(S) &= A^+(P_+P_-) = A_{-+}(P_+, P_-) + A_{++}(-P_+, P_-) \\ &= A_{-+}(S) + A_{++}(-S) \end{aligned} \tag{1.1}$$

with

$$A_{-+}(S) \underset{S \rightarrow \infty}{\rightarrow} c S, \quad A_{++}(S) \underset{S \rightarrow \infty}{\rightarrow} -c S \tag{1.2}$$

In a vector theory the amplitudes $A_{-+}(S)$ and $A_{++}(S)$ would simply add in a single helicity amplitude and the anomaly would cancel.

We will show that at $O(\alpha_s)$ the anomaly is already present. It is generated by the combination of an effective vertex due to the left-handed coupling of a scattering vector meson, a quark-antiquark effective vertex due to a longitudinal massive vector intermediate state, and a single (large transverse momentum) gluon vertex. At $O(\alpha_s)$, there is only a small number of possibilities for the anomaly to occur, within the transverse momentum diagram formalism, and it is clear that it does not cancel. At $O(\alpha_s^2)$ there are contributions in which an additional soft gluon plays no kinematical role in the occurrence of the anomaly and simply accompanies the $O(\alpha_s)$ process. Not surprisingly, the soft gluon produces a transverse momentum infra-red divergence in individual diagram contributions. In tracing the corresponding cancelation, we find

new (but closely related) processes which occur first only at $O(\alpha_s)^2$ and for which infra-red properties of the anomaly are needed to fully determine their contribution.

Also at $O(\alpha_s^2)$, “anomalous” (odd) color charge parity two gluon exchange appears, involving one finite and one large transverse momentum gluon. In this paper we will frequently refer to a multigluon transverse momentum state which carries color zero and anomalous color charge parity (not equal to the gluon number) as “anomalous gluons”. In the present context, such a state first appears at $O(\alpha_s^3)$. Three gluons with even color parity and (separately) large, finite, and soft transverse momentum are involved. In higher orders various combinations of soft and finite transverse momentum gluons can accompany the large transverse momentum gluon. Additional gluons could also share the large transverse momentum, but we do not discuss this possibility.

Reggeized gluon exchanges that are the outcome of perturbative calculations[1]-[7] in a vector theory carry normal color parity (even/odd for an even/odd number of gluons). However, we have argued (for a very long time[10]) that anomalous gluons play a crucial role[8] in the emergence of QCD confinement and chiral symmetry breaking, in the context of high-energy scattering and reggeon diagrams. In particular, we have argued that the pomeron is formed from anomalous gluons and that configurations of this kind are an essential component of regge limit pions and nucleons. However, while we have been able to show how[9] anomalies provide triple pomeron and pion/pomeron interactions involving the anomalous gluons, it has proven very difficult to find a simple starting point in which the anomalous gluons couple directly and from which a detailed description of hadron amplitudes can be developed. It is very encouraging, therefore, to see that anomalous gluons appear straightforwardly in the anomaly contributions that dominate the electroweak scattering amplitudes we consider.

We have not explored the full consequences of the power enhancement (1.2) nor, as we discussed above, is it clear that the possibilities for cancelation have been exhausted. While no unitarity bound is violated, we, nevertheless, believe that the enhancement severely threatens the unitarity of the theory (at least in the t - channel) and should not be present in physical amplitudes. Rather than looking for further cancelations, we will argue (only very briefly in this paper) that although the enhancement is actually unphysical, it selects the physically relevant diagrams and, in doing so, anticipates chiral symmetry breaking and confinement. In fact there is no sign, in the anomaly amplitudes that give (1.2), of either the s - channel or the t - channel intermediate states that are present in the diagrams from which they are calculated. We will suggest that the enhancement is obtained by using a “wrong procedure” to evaluate the regge limit contribution of diagrams. If a transverse momentum cut-off is initially imposed, the energy enhancement will be eliminated. Instead, because the cut-off produces a Ward identity violation, the anomaly diagrams dominate because

of infra-red transverse momentum divergences that appear and infra-red properties of the anomaly come into play. We will argue that these divergences should be analysed, and “physical amplitudes” extracted, before the cut-off is removed.

To begin with, a study of the infra-red anomaly contributions of diagrams, that matches the present study of ultra-violet contributions, will be required. After this, we anticipate, the analysis of infra-red divergences will parallel our discussion[8] of hadron scattering. All-orders properties of the divergences have to be combined with Reggeon Field Theory, to obtain the “physical amplitudes” in which the cut-off can be removed. In this paper we will describe only the general arguments that we believe should be employed. We expect that the resulting amplitudes will have both confinement and chiral symmetry breaking, in the sense that the scattering will be describable as the exchange of a color zero, Goldstone boson, pion. Although our hadron work provides the framework for our general understanding, a major part of the logic and justification for the procedure we outline can be appreciated directly within the present context, without reference to the pomeron problem. That the starting point is much more straightforward than in the hadron case holds out the promise that it will be correspondingly easier to carry the procedure through in detail.

2. THE ALMOST STANDARD MODEL

For simplicity, we will consider a theory which, for our purposes, is sufficiently close to the Standard Model, but which is actually less complex. We will consider a “flavor SU(2)” triplet of vector mesons $\{W^+, W^-, W^0\}$ with mass M and left-handed couplings to a flavor doublet of quarks $\{u, d\}$ with the usual QCD interaction. We will effectively assume that the vector mesons originate from a spontaneously-broken gauge theory, as in the Standard Model, but apart from the discussion of reggeization in this Section, their self-interaction will play almost no role in our analysis. (There will be no gauge dependence in our discussion because the vector mesons will always be on-shell and gluons will only contribute in gauge-independent transverse momentum diagrams - although, in effect, we evaluate gluon contributions in Feynman gauge.)

We ignore the extra complications of the photon and all mixing angles, which could only lessen the possibilities for cancelation of the anomaly phenomenon that we find. Since there is no photon, the usual electroweak ultraviolet anomaly is absent and so we do not need to include leptons. In fact, as we noted in the Introduction, the anomaly we discuss involves (components of) QCD currents to which leptons do not couple and, therefore, could not provide any possibility for cancelation. If we give the quarks a small mass m ($\ll M$) any potentially singular infra-red contributions will be eliminated. However, for much of our discussion we will be interested only in large internal (transverse) momenta, where “large” is defined relative to M , and so m will be omitted. The absence of a quark mass has the technical advantage that we will be able to exploit the considerable, regge limit, simplifications of the feynman diagrams that describe a massless, chiral, theory.

We will study the high-energy scattering of the massive vector mesons via a quark-antiquark exchange channel in which, potentially, a “pion” could appear as a bound state. Perturbatively, the leading behavior of the amplitudes we study would be given (if there were no anomaly enhancement) by the exchange of vector mesons. However, since the flavor symmetry is non-abelian, the vector mesons will be reggeized by self-interactions. Since CP is conserved, signature is well-defined and reggeized vector meson exchange will give high-energy behavior in the odd-signature channel of the form

$$A(S, 0) \underset{S \rightarrow \infty}{\sim} S^{\alpha(0)} \quad (2.1)$$

where

$$\alpha(0) = 1 - \frac{g^2}{16\pi^2} + O(g^4) < 1 \quad (2.2)$$

The even signature channel will be dominated by the exchange of two reggeized vector

mesons for which (apart from a logarithmic factor)

$$A(S, 0) \underset{S \rightarrow \infty}{\sim} S^{2\alpha(0)-1} < S^{\alpha(0)} \quad (2.3)$$

Therefore, if we sum (in principle at least) all diagrams producing all self-interaction reggeization effects then the contribution of (any number of) exchanged vector mesons to flavor exchange amplitudes will be smaller than the anomaly enhanced quark-antiquark exchange amplitudes we discuss which give

$$A(S, 0) \underset{S \rightarrow \infty}{\sim} \frac{S}{M^2} \quad (2.4)$$

Since the running of α_s does not enter our calculations, the relative value of M , compared to the QCD scale, does not appear in our discussion. Therefore, the instability of the vector mesons is not an issue. More generally it also should not be a very significant issue. We can, of course, define vector meson scattering amplitudes by going to complex poles and any undesirable features of these amplitudes will feed back into the scattering amplitudes of physical particles. Alternatively, we could exploit the reggeization property of vector mesons and, although it would be very obscure for most readers, we could carry out our discussion in terms of reggeon amplitudes. In this case, it would be rather straightforward to argue that the non-regge nature of the anomaly enhancement energy behavior that we find will violate t - channel unitarity. However, since the simplest diagrams we consider are already very high-order in the electroweak coupling ($O(\alpha_w^4)$) their contribution is very small at current energies and so any unitarity problems could only be of physical relevance at extremely high energies.

We could also regard our calculations as academic and say that we are simply using left-handed vector mesons to uncover properties of QCD. From this point of view we could make the mass M as small as we like. Also, throughout the main body of the paper the origin of M will be irrelevant and we will implicitly assume that it originates from some mechanism which is unrelated to the quarks we consider. It is important that the high-energy behavior (2.4) is obtained with internal vector mesons on mass-shell. Because longitudinal states are involved this behavior is scaled by M^2 and so can not be canceled by a physical Higgs contribution of any kind.

If we ignore reggeization, or if the vector mesons are massless, then the anomaly enhanced amplitudes will give high-energy behavior comparable with that of (multiple) vector meson exchange. This could be an additional reason, to be added to those briefly mentioned in Section 5, why bound-states of (higher-colored) quarks and antiquarks should actually be responsible for the vector meson mass generation. If the electroweak scale M is actually a second QCD scale, as would then be the case, we would surely expect unitarity to be just as important for the higher scale as for the lower scale.

3. $O(\alpha_s)$ - ONE GLUON DIAGRAMS

As is very well known, the leading (regge limit) high-energy behavior of a feynman diagram is typically obtained by routing the large light-cone momenta through the diagram in such a way that the number of particles that are close to mass-shell and have large, relative, longitudinal momentum separations (i.e. large rapidity differences) is maximal. After longitudinal integrations are carried out, close to the on-shell configuration, the result is a transverse momentum integral multiplied by logarithms of the energy. The transverse momentum integral corresponds to a “transverse momentum diagram” obtained by contracting all of the (close to) on-shell lines. In general, there is one logarithm and one transverse momentum loop for each large rapidity difference. Consequently, the leading-log amplitude contains a transverse momentum diagram with the maximal number of loops.

The relationship between transverse momentum diagrams and the process of putting lines on-shell in full feynman diagrams will dominate our discussion. When two, or more, particles have finite relative rapidity, fewer lines are placed on-shell in the reduction to a transverse momentum diagram, and a non-leading log amplitude, with a smaller number of transverse momentum loops, is obtained. In this case, the couplings and interactions in the transverse momentum diagrams have more structure. It is in (superficially) non-leading amplitudes of this kind that the high-energy behavior can be enhanced by the occurence of the triangle anomaly within the couplings of the transverse momentum diagram.

In Appendix B we provide a brief, non-technical, review[11] of known results that apply to the fermion exchange scattering amplitudes we will discuss. A well-known extra complication, in the application of the transverse momentum diagram formalism to such amplitudes, is that transverse momentum loops involving only fermion propagators are generally logarithmically divergent[11] at large transverse momentum. These divergences, effectively, produce additional logarithms of the energy and give rise to “double logs” that are associated with single rapidity differences. In the diagrams we discuss there is, potentially, a logarithmic divergence of this kind but it is overwhelmed by the anomaly power divergence that we find. Therefore, we will not be directly interested in logarithmic transverse momentum divergences and, in the main body of the paper, will refer to them only for reasons of completeness. In Appendix B we briefly discuss the possible physical relevance of the anomaly with respect to the double logs.

From the general viewpoint of this paper, however, it is important that, because we can regard the double logs as described by transverse momentum diagrams, there is no high-energy behavior that is not anticipated by this formalism. (Even though it might not be the most efficient method for studying properties of the dou-

ble logs.) It is, perhaps, worth noting that, since the divergences do not occur in reggeization diagrams, they do not affect the reorganization of transverse momentum diagrams into reggeon diagrams. In fact, this reorganization reduces the degree of divergence. The divergences occur only in reggeon diagram loops containing just reggeized quarks and antiquarks and, if the leading log form of the trajectory function is used, the presence of the reggeon propagator reduces the divergence from \log to $\log[\log]$ form.

3.1 The Transverse Momentum Diagram

The remainder of this Section will be devoted to the study of $O(\alpha_s)$ feynman diagrams which give a contribution to the high-energy scattering of vector mesons that contains the transverse momentum integral shown in Fig. 1.

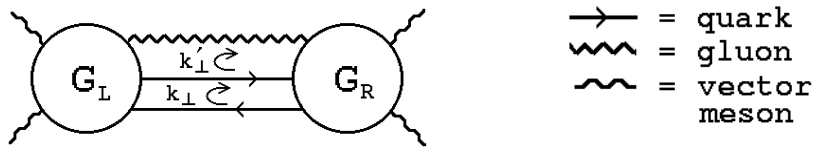


Fig. 1 A Transverse Momentum Diagram

We will use the diagrammatic notation of Fig. 1 - for quarks, gluons, and vector mesons - throughout the paper, in both feynman diagrams and transverse momentum diagrams. (Almost all of our discussion will be concerned with feynman diagrams and so there should be no confusion as to which kind of diagram is under consideration.) In this Section only, however, we omit flavor and color quantum numbers and consider just the momentum and spin structure of diagrams. For this purpose, therefore, a “gluon” is effectively a “photon”, i.e. a massless vector particle with a vector coupling to a massless (for most of the discussion) “quark-antiquark” pair. A “vector meson” is a massive vector particle with a left-handed (right-handed) coupling to the quark (antiquark). Because of the left-handed coupling, the high-energy scattering of vector bosons with definite helicity has a particularly simple diagrammatic structure.

To avoid the introduction of an extra momentum scale, we will consider forward scattering, i.e. zero momentum transfer. We should emphasize, however, that this does not imply that our calculations are invalidated for the simple reason that we consider an infra-red region in which perturbation theory does not apply. It should become clear that, since the phenomenon we discuss involves large internal transverse momenta, a momentum transfer t with $M^2 \ll t \ll S$ would not significantly affect our analysis. In the forward direction, the integrand of Fig. 1 is a product of the

couplings $G_L(k_\perp, k'_\perp)$ and $G_R(k_\perp, k'_\perp)$ and transverse momentum propagators for the gluon, quark, and antiquark and the integral has the simple form

$$\int d^2 k'_\perp \int d^2 k_\perp \frac{\text{Tr} \{ \not{k}_\perp G_L(k_\perp, k'_\perp) \not{k}_\perp G_R(k_\perp, k'_\perp) \}}{k'^2 (k_\perp^2)^2} \quad (3.1)$$

The G_L and G_R should satisfy (reggeon) Ward identities so that, as discussed further in Section 5, there is no infra-red divergence at $k'^2 = 0$ and a divergence at $k^2 = 0$ would be eliminated by adding either a momentum transfer or a quark mass, as discussed in the previous Section. Conventionally, since two fermion exchange is involved, we would expect the accompanying energy dependence to be only logarithmic. We would also expect the large momentum behavior of G_L and G_R to be such that the full integral is, at worst, logarithmically divergent (producing an additional energy logarithm, as discussed above). The signal of the anomaly will be that G_L and G_R actually grow at large transverse momentum, leading to a power divergence that produces an additional power of the energy.

3.2 The Simplest Graph Containing the Anomaly Enhancement

We begin by considering the feynman graph shown in Fig. 2.

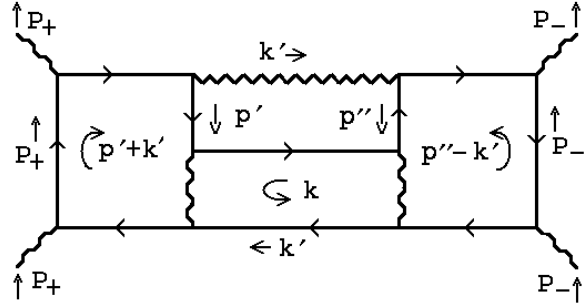


Fig. 2 The Simplest Graph

We label the momenta as shown and consider the limit

$$P_+ \rightarrow \left(\frac{\sqrt{S}}{2}, \frac{\sqrt{S}}{2}, 0, 0 \right), \quad P_- \rightarrow \left(\frac{\sqrt{S}}{2}, -\frac{\sqrt{S}}{2}, 0, 0 \right) \quad (3.2)$$

As we will see below, in this limit, the diagram of Fig. 2 contributes to the scattering of vector mesons with opposite helicities and does not contribute to same sign helicity amplitudes. A simple way to see this is to note that the leading behavior originates when the left side quark and right side antiquark are close to mass-shell. (In Fig. 3, below, these lines are actually on-shell.) Consequently, the left side scattering vector

boson has to make a transition to a left-handed intermediate state quark and so must carry negative ($\lambda = -1$) helicity. Similarly, the right side scattering vector boson must make a transition to a right-handed antiquark and so must carry positive ($\lambda = +1$) helicity.

We focus on the particular graph shown in Fig. 2 because we anticipate that there will be a high-energy contribution, involving the transverse momentum diagram of Fig. 1, in which the hatched lines of Fig. 3 are placed on-shell.

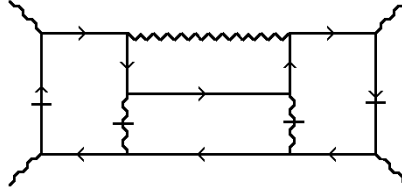


Fig. 3 On-shell Lines for the Anomaly Contribution

With lines on-shell as in Fig. 3, the box graphs at either end of the full graph contract to give triangle diagram contributions to the couplings, G_L and G_R , as shown in Fig. 4. The left-handed nature of the interactions of the scattering vector particles leads to a left-handed vector (“effective”) vertex for the triangle diagram that potentially produces the triangle anomaly. To obtain a non-zero contribution in the full amplitude, it will be necessary to have the anomaly appear in both the right and left-side couplings. The diagram of Fig. 2 has the minimal complexity for this to be the case.

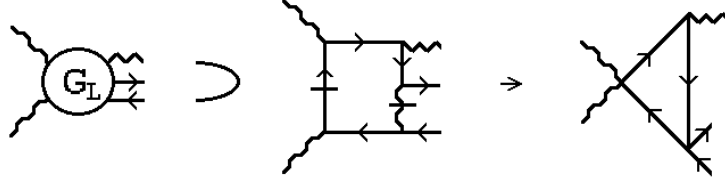


Fig. 4 A Triangle Diagram Effective Coupling

3.3 Comparison with Leading and Non-Leading Log Amplitudes

A priori, as described in Appendix B, we expect the leading high-energy behavior of Fig. 2 to be $[\ln s]^4$, multiplied by the transverse momentum diagram obtained, as illustrated in Fig. 5, by placing all vertical lines on-shell.

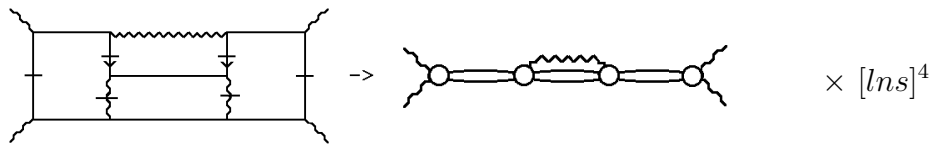


Fig. 5 The Leading-Log Amplitude

(A hatch on a line will always imply that it is on-shell.) In fact, this transverse momentum diagram contains quark loops that are logarithmically divergent and so there will be extra powers of $\ln s$, as we have discussed above.

The transverse momentum diagram of Fig. 1 should appear (formally) with a factor of $[\ln S]^2$, i.e. at the next-to-next-to-leading log level. Also, in this contribution, the dominant internal momenta within the G_L and G_R couplings, should be “close to” that of the corresponding fast external particle (in particular, there should be no large internal rapidity difference.) Consequently, all the hatched lines of Fig. 5 should remain close to on-shell.

A priori, we expect that large (relative) internal momenta within the G_L and G_R couplings, that give a worse than logarithmically divergent integral, will be suppressed because of Ward identity cancelations that are a consequence of gauge invariance for the gluon. As we will see, the anomaly contradicts this expectation in that it is a contribution to the G_L and G_R couplings from, relatively, large internal momentum in which the unhatched vertical quark lines of Fig. 3 (and, correspondingly, the unhatched vertical line of Fig. 4) are far off-shell. However, this does not imply the failure of a Ward identity. Rather, as we enlarge on further in Section 5, the presence of the anomaly means that large internal momenta play an important role in the Ward identity. (In Appendix C we review the corresponding situation for the vector Ward identities in the familiar axial-vector/vector/vector triangle diagram in which the anomaly occurs.)

In the course of our analysis we will find that, in the low-order diagrams where the anomaly first occurs, there are no additional logarithms multiplying the power enhancement associated with the large transverse momentum divergence.

3.4 Internal Momenta and the Quark Mass-Shell Conditions

Consider, first, the left-hand box sub-graph of Fig. 3 that appears in Fig. 4. We direct P_+ along the left-most quark line, as shown in Fig. 2, and use the k'_- integration to put this line on-shell, i.e.

$$\int dk'_- \frac{i \gamma \cdot (P_+ + \dots)}{(k'_- + p'_-) P_+ + i\epsilon + \dots} \xrightarrow[P_+ \rightarrow \infty]{} \pi \gamma_- + \dots \quad (3.3)$$

We focus on that part of the p' integration in which

$$|p'_+| \sim \epsilon S^{\frac{1}{2}} \ll P_+, \quad {p'_\perp}^2 \sim \epsilon M S^{\frac{1}{2}} \ll M P_+, \quad |p'_-| \sim \epsilon M \quad (3.4)$$

where ϵ is small, but finite. If, as we will impose in the following,

$${k'_\perp}^2 \sim \epsilon^{\frac{3}{2}} M S^{\frac{1}{2}} \ll {p'_\perp}^2 \quad (3.5)$$

then the mass-shell condition (3.3) requires that

$$|k'_- + p'_-| \sim \frac{p'_\perp^2}{P_+} \sim \frac{\epsilon M S^{\frac{1}{2}}}{S^{\frac{1}{2}}} \sim \epsilon M \quad (3.6)$$

which, together with (3.4), implies that $|k'_-| \sim \epsilon M$. The powers of ϵ , in (3.4) and (3.5), and in the following, provide a simple way to impose inequalities amongst the momenta involved that we could have imposed more abstractly. Since we are only interested in showing that an anomaly power enhancement occurs, and will make no attempt to determine the coefficient multiplying it, the use of powers of ϵ will be sufficient to carry through our arguments.

If we similarly direct P_- along the right-most quark line in Fig. 2 and consider the analogous region of the p'' integration, then using k'_+ to put this line on-shell we will obtain a similar constraint on k'_+ . Together, these constraints ensure that, in the momentum region we are considering, transverse momenta dominate the gluon propagator. (3.4) and (3.5), together with the corresponding range for p'' , define a range of internal transverse momenta that is growing with the external energy but which is, nevertheless, close to mass-shell for the hatched quark lines.

3.5 Adjacent Quark Numerators and the External Effective Vertices

Consider, next, the contribution of the quark numerators that are adjacent to the fast quark line. When combined with (3.3), the γ_- components give zero. Therefore, the leading contribution, in the momentum region we are considering, is given by the transverse numerator components. To discuss this contribution we use the complex γ - matrix formalism[16] described in Appendix A. We can then write both numerators in the form

$$\not{p}_\perp = \frac{1}{2} [(\hat{p}' + \hat{k}') \hat{\gamma}^* + (\hat{p}' + \hat{k}')^* \hat{\gamma}] \quad (3.7)$$

We take the vector meson states to be transversely polarized. The helicity of each vector meson will be conserved, but the two helicities can be equal or opposite. Using (A.13) and (A.14), the $(1 - \gamma_5)$ vector meson coupling implies that, as illustrated in Fig. A1, there is just one combination of $\hat{\gamma}$ and $\hat{\gamma}^*$ numerator matrices that can contribute for each helicity. For helicity $\lambda = -1$, the resulting coupling is that illustrated in Fig. 6(a), while $\lambda = +1$ gives that of Fig. 6(b).

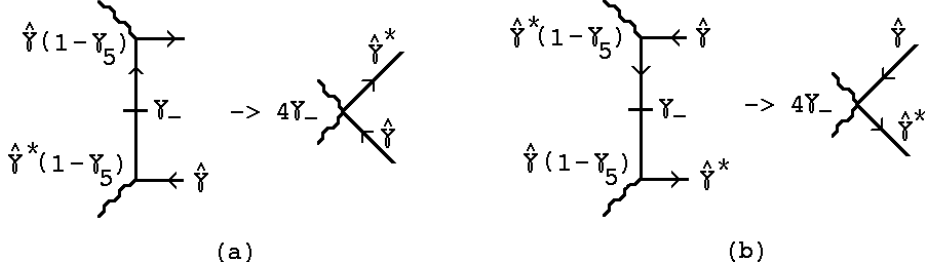


Fig. 6 Effective Vertices (a) for Helicity $\Lambda = -1$ (b) for Helicity $\Lambda = +1$

(In all the figures of this kind we follow the normal convention and multiply γ -matrices in the direction of the quark arrow.)

3.6 The Internal Vector Mesons

The on-shell contribution of the internal vector meson propagator is, of course, gauge independent and can be obtained from the unitary gauge propagator

$$\Gamma_{\mu\nu}(p' + k) = \frac{(g_{\mu\nu} - (p' + k)_\mu(p' + k)_\nu/M^2)}{(p' + k)^2 - M^2} \quad (3.8)$$

It is the second part of the on-shell numerator, corresponding to longitudinal polarization of the intermediate state, that produces[8] the vector-like (cross-channel) coupling needed to obtain the anomaly. We will obtain a (large) factor of p'_+ in this part of the numerator if there is a γ_- at one of the vertices. This is only possible at the upper vertex in Fig. 4, since a γ_- at the bottom vertex would (anti-)commute through the adjacent transverse numerator and give zero.

If $k_\perp^2 \gg p'_\perp^2$, which is satisfied if

$$k_\perp^2 \sim \epsilon^{\frac{1}{2}} M S^{\frac{1}{2}} \quad (3.9)$$

then, with the γ_- present, the dominant contribution of the vector meson numerator is as shown in Fig. 7. (We remove the $(1 - \gamma_5)$ factors in the quark couplings of the internal vector meson by (anti-)commuting them around the quark loop.)

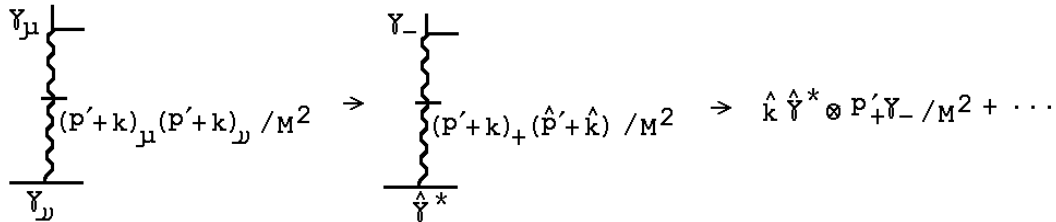


Fig. 7 The Internal Vector Meson Numerator

The \otimes notation indicates that the two γ -matrices are not multiplied.

Putting the vector meson propagator on-shell via the k_- integration gives

$$\int dk_- \frac{(\hat{k}\hat{\gamma}^* \otimes i p'_+ \gamma_- + \dots)/M^2}{[(k_- + p'_-) p'_+ \dots]} \quad p'_+ \xrightarrow{\sim} \infty \quad \pi \hat{k}\hat{\gamma}^* \otimes \gamma_- / M^2 \quad (3.10)$$

and, if (3.9) is satisfied, the mass-shell constraint gives

$$|k_-| \sim \frac{k_\perp^2}{|p'_+|} \sim \frac{\epsilon^{\frac{1}{2}} M S^{\frac{1}{2}}}{\epsilon S^{\frac{1}{2}}} \sim \epsilon^{-1/2} M \quad (3.11)$$

The parallel discussion of the on-shell contribution of the right-side internal vector meson will give a corresponding constraint on $|k_+|$. The two constraints, taken together with (3.9), imply that (as for the gluon) transverse momenta dominate the central quark and antiquark propagators. Note that, although we consider very large transverse momenta, because the vector mesons remain on-shell the high-energy behavior we will find will be scaled by M^2 . Consequently, there is no possibility that it could be canceled by the contribution of a Higgs particle. (That is, if the Higgs mechanism were used to generate the vector meson mass.)

3.7 The Internal Quark Numerator and the Triangle Amplitude

For the remaining components of Fig. 4 that we have not yet discussed, the largest contribution, giving the γ_- - coupling vertex of Fig. 7, is obtained by taking the gluon coupling to be γ_+ and taking the remaining quark numerator to also be transverse. The chirality then feeds through the propagator as illustrated in Fig. 8.

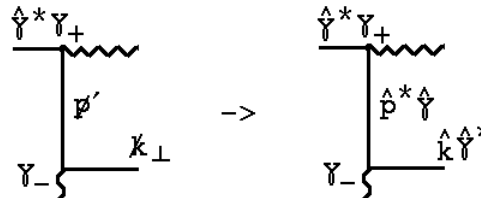


Fig. 8 The Internal Quark Numerator

Combining Figs. 6, 7, and 8, and using (3.10) we obtain an effective triangle diagram with the numerators and vertices shown in Fig. 9. In this figure we have also included the transverse quark and antiquark propagators ($\hat{\gamma}/\hat{k}$ and $\hat{\gamma}^*/\hat{k}^*$) that are external to the triangle diagram.

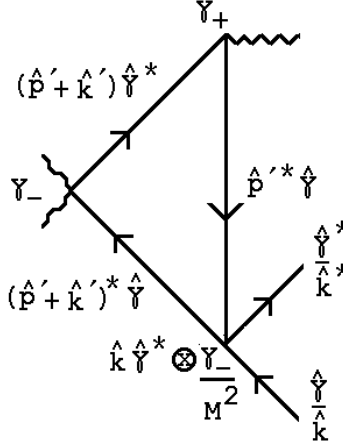


Fig. 9 The Effective Triangle Diagram

The amplitude obtained from Fig. 9 is (apart from an overall constant involving a numerical factor, factors of π , and powers of the coupling constants, that we neglect)

$$\frac{\hat{\gamma}}{\hat{k}} G_L(k_{\perp}, k'_{\perp}) \frac{\hat{\gamma}^*}{\hat{k}^*} \sim \frac{\hat{\gamma}}{\hat{k}} \left(\int d^4 p' \frac{\hat{k} \hat{\gamma}^* (\hat{p}' + \hat{k}')^* \hat{\gamma} \gamma_- (\hat{p}' + \hat{k}') \hat{\gamma}^* \gamma_+ [\hat{p}']^* \hat{\gamma}}{(p' + k')^4 (p')^2} \frac{\gamma_-}{M^2} \right) \frac{\hat{\gamma}^*}{\hat{k}^*} \quad (3.12)$$

with the integration region specified by (3.4).

From (3.4)-(3.6),

$$\begin{aligned} |k'_+ (p'_- + k'_-)| &\sim \epsilon^2 M^2, \\ |p'_+ (p'_- + k'_-)| &\sim \epsilon^2 M S^{\frac{1}{2}}, \\ (p' + k')_{\perp}^2 &\sim (\epsilon + O(\epsilon^{\frac{5}{4}})) M S^{\frac{1}{2}} \end{aligned} \quad (3.13)$$

and so

$$(p' + k')^2 \sim (p' + k')_{\perp}^2 \quad (3.14)$$

Consequently, we can approximate (3.12) as (again ignoring an overall constant)

$$\frac{\hat{\gamma}}{\hat{k}} G_L(k_{\perp}, k'_{\perp}) \frac{\hat{\gamma}^*}{\hat{k}^*} \sim \frac{\hat{\gamma}}{\hat{k}} \left(\int d^4 p' \frac{\hat{k} [\hat{p}']^*}{[p'_{\perp} + k'_{\perp}]^2 [2p'_+ p'_- - (p'_{\perp})^2]} \frac{\gamma_-}{M^2} \right) \frac{\hat{\gamma}^*}{\hat{k}^*} \quad (3.15)$$

with the integration region still specified by (3.4). Because we have eliminated k'_- and k'_+ (which are functions of p' and p''), the amplitude (3.15) is (almost) that of a conventional triangle feynman diagram - with local vertices.

3.8 The Anomaly Contribution

Using (A.4) we can write the numerator momentum factor of (3.15) as

$$\hat{k} [\hat{p}']^* = k_{\perp} \cdot p'_{\perp} + i k_{\perp} \times p'_{\perp} \quad (3.16)$$

The first term is not special to a vector vertex fermion triangle diagram and is not related to the anomaly. We expect it to arise from (and to eventually be canceled by) a variety of contributions to the complete transverse momentum couplings of Fig. 1. It is the second term in (3.16) that we expect to give an anomaly contribution. Its parity properties result directly from the product of an odd number of quark numerators and so we anticipate that it can only be canceled by effective triangle diagrams that contain three quark propagators.

Keeping just the second term in (3.15) gives, for the integral within the brackets (apart from the factor of γ_-/M^2)

$$\int dp'_+ dp'_- \int d^2 p'_\perp \frac{i k_\perp \times p'_\perp}{[p'_\perp + k'_\perp]^2 [2p'_+ p'_- - (p'_\perp)^2]} \quad (3.17)$$

To carry out the angular integration for p'_\perp we choose co-ordinates (p'_2, p'_3) such that k'_\perp lies along the 2-axis. In this case,

$$p'_\perp \cdot k'_\perp = |p'_\perp| |k'_\perp| \cos\phi, \quad p'_\perp \times k_\perp = |p'_\perp| (k_3 \cos\phi - k_2 \sin\phi) \quad (3.18)$$

where k_2 and k_3 are projections of k_\perp along and perpendicular to k'_\perp . We can, therefore, write

$$\begin{aligned} & \int dp'_+ dp'_- \int \frac{d(p'_\perp)^2}{[2p'_+ p'_- - (p'_\perp)^2]} \frac{k_\perp \times p'_\perp}{[p'_\perp + k'_\perp]^2} \\ &= \int dp'_+ dp'_- \int \frac{d(p'_\perp)^2}{[2p'_+ p'_- - (p'_\perp)^2]} \int_0^{2\pi} d\phi \frac{|p'_\perp| (k_3 \cos\phi - k_2 \sin\phi)}{[(p'_\perp)^2 + (k'_\perp)^2 + 2|p'_\perp| |k'_\perp| \cos\phi]} \end{aligned} \quad (3.19)$$

Using

$$\int_0^{2\pi} d\phi \frac{\sin\phi}{a + b \cos\phi} = -\frac{1}{b} [a + b \cos\phi]_0^{2\pi} = 0 \quad (3.20)$$

and

$$\begin{aligned} \int_0^{2\pi} d\phi \frac{\cos\phi}{a + b \cos\phi} &\underset{b \ll a}{\sim} \frac{1}{a} \int_0^{2\pi} d\phi \cos\phi - \frac{b}{a^2} \int_0^{2\pi} d\phi \cos^2\phi + O\left(\left[\frac{b^2}{a^3}\right]\right) \\ &\sim 0 - \frac{\pi b}{a^2} + O\left(\left[\frac{b^2}{a^3}\right]\right) \end{aligned} \quad (3.21)$$

we obtain

$$\int d\phi \frac{k_\perp \times p'_\perp}{[p'_\perp + k'_\perp]^2} \underset{k'_\perp{}^2 \ll p'_\perp{}^2}{\sim} \frac{k_3 |k'_\perp|}{p'_\perp{}^2} \underset{k'_\perp{}^2 \ll p'_\perp{}^2}{\sim} \frac{k_\perp \times k'_\perp}{p'_\perp{}^2} \quad (3.22)$$

(3.19) gives, therefore,

$$k_\perp \times k'_\perp \int_{p'_\perp^2 \sim \epsilon M \sqrt{S}} \frac{d(p'_\perp^2)}{(p'_\perp^2)} \int_{|p'_+| \sim \epsilon \sqrt{S}, |p'_-| \sim M} \frac{dp'_+ dp'_-}{[2p'_+ p'_- - (p'_\perp)^2]} \quad (3.23)$$

If we change variables to

$$\sqrt{S} x = p'_\perp^2, \quad \sqrt{S} y = p'_+ \quad (3.24)$$

we obtain

$$\begin{aligned} & \int_{p'_\perp^2 \sim \epsilon M \sqrt{S}} \frac{d(p'_\perp^2)}{(p'_\perp^2)} \int_{|p'_+| \sim \epsilon \sqrt{S}, |p'_-| \sim M} \frac{dp'_+ dp'_-}{[2p'_+ p'_- - (p'_\perp)^2]} \\ &= \int_{x \sim \epsilon M} \frac{dx}{x} \int_{|y| \sim \epsilon, |p'_-| \sim \epsilon M} \frac{dy dp'_-}{[2y p'_- - x]} \end{aligned} \quad (3.25)$$

which is clearly a constant - that we do not need to evaluate. (3.23) is sufficient to conclude that the integration region on which we have focussed gives, for (3.15), the behavior

$$\sim \frac{\hat{\gamma}^*}{\hat{k}^*} \left(\frac{(k_\perp \times k'_\perp) \gamma_-}{M^2} \right) \frac{\hat{\gamma}}{\hat{k}} \quad (3.26)$$

3.9 Behavior of the Full Amplitude

It is straightforward to obtain the behavior of the full amplitude that results from combining (3.26) with the corresponding contribution from the right-side box graph in Fig. 3. As we have discussed above, the internal mass-shell conditions determine that the longitudinal momenta in the central propagators of Fig. 3 can be neglected. As a result the k'_\perp and k_\perp loop integrations produce, as anticipated, a transverse momentum integral of the form of (3.1) which we write, in complex γ - matrix notation, as

$$\begin{aligned} & \int \frac{d^2 k'_\perp}{k'_\perp^2} \int d^2 k_\perp \text{Tr} \left\{ \frac{\hat{\gamma}}{\hat{k}} G_L(k_\perp, k'_\perp) \frac{\hat{\gamma}^*}{\hat{k}^*} G_R(k_\perp, k'_\perp) \right\} \\ & \sim \int \frac{d^2 k'_\perp}{k'_\perp^2} \int d^2 k_\perp \left(\frac{k_\perp \times k'_\perp}{M^2} \right)^2 \frac{\text{Tr}\{\gamma_- \hat{\gamma}^* \gamma_+ \hat{\gamma}\}}{\hat{k} \hat{k}^*} \\ & \sim \int \frac{d^2 k'_\perp d^2 k_\perp}{k'_\perp^2 k_\perp^2} \left(\frac{k_2 k'_3 - k_3 k'_2}{M^2} \right)^2 \\ & \sim \frac{1}{M^4} \int^{O(MS^{\frac{1}{2}})} d(k'_\perp^2) \int^{O(MS^{\frac{1}{2}})} d(k_\perp^2) \sim \frac{S}{M^2} \end{aligned} \quad (3.27)$$

As we noted above, because two fermion exchange is involved, we would have expected the amplitude to increase only as some power of $\ln S$. However, we have now shown that the kinematic region of Fig. 3 that we have isolated actually produces a power enhancement of the expected high energy behavior. As we will see shortly, there are no accompanying logarithms in this lowest-order appearance of the anomaly.

Because the anomaly contribution to $G_L(k_\perp, k'_\perp)$ is linear in k'_\perp , if it is combined with a $G_R(k_\perp, k'_\perp)$ that does not have this contribution then integration over k'_\perp will give a cancellation of the enhancement effect. This is why we considered a diagram which gives anomaly contributions to both G_L and G_R .

3.10 Comparison With the Axial Vector Vertex Anomaly

To see the relationship between the anomaly amplitude (3.26) that we have found and the familiar axial vector anomaly we proceed as follows. First we change variables from p' to q where

$$q_+ = \frac{p'_+}{\Lambda}, \quad q_- = \Lambda p'_-, \quad q_\perp = p'_\perp, \quad \Lambda = \left(\frac{\epsilon}{M}\right)^{\frac{1}{2}} S^{\frac{1}{4}} \quad (3.28)$$

If we also extend the integration region for p'_- to $p'_- \sim M$ (which would not significantly alter the above analysis) then (3.15) becomes (moving the γ_-/M^2 outside of the brackets)

$$\frac{\hat{\gamma}}{\hat{k}} \left(\int_{|q_j| \sim (\epsilon M)^{\frac{1}{2}} S^{\frac{1}{4}}} dq_j \frac{\hat{k} \hat{q}^*}{[q_\perp + k'_\perp]^2 [2q_+ q_- - q_\perp^2]} \right) \frac{\gamma_-}{M^2} \frac{\hat{\gamma}^*}{\hat{k}^*} \quad (3.29)$$

where, as indicated the range of integration is now the same for all components of q . In the limit $S \rightarrow \infty$, the integration is over a four-dimensional large momentum region and, formally, the integral is linearly divergent. Also, a product of three orthogonal γ matrices is present - although there is no trace involved. Consequently, it is natural to expect a large momentum contribution of the form associated with the triangle anomaly.

The strictly infinite momentum region contribution to (3.29) is

$$\sim \frac{\hat{\gamma}}{\hat{k}} \left(\int dq_+ dq_- \int d^2 q_\perp \left[\frac{k_\perp \times q_\perp}{q_\perp^2} \right] \frac{1}{[2q_+ q_- - q_\perp^2]} \right) \frac{\gamma_-}{M^2} \frac{\hat{\gamma}^*}{\hat{k}^*} \quad (3.30)$$

which, integrating by parts with respect to q_\perp^2 , we can rewrite as

$$\sim \frac{\hat{\gamma}}{\hat{k}} \left(\int dq_+ dq_- \int d^2 q_\perp \frac{k_\perp \times q_\perp}{[2q_+ q_- - q_\perp^2]^2} \right) \frac{\gamma_-}{M^2} \frac{\hat{\gamma}^*}{\hat{k}^*} \quad (3.31)$$

and, with a further integration by parts, as

$$\sim \frac{\hat{\gamma}}{\hat{k}} \left(\int dq_+ dq_- \int d^2 q_\perp \frac{q_\perp^2 [k_\perp \times q_\perp]}{[2q_+ q_- - q_\perp^2]^3} \right) \frac{\gamma_-}{M^2} \frac{\hat{\gamma}^*}{\hat{k}^*} \quad (3.32)$$

Undoing the γ - matrix removal involved in going from (3.12) to (3.15) (or, equivalently, inserting γ - matrices using $2 = \gamma_+ \gamma_- + \gamma_- \gamma_+ = \hat{\gamma} \hat{\gamma}^* + \hat{\gamma}^* \hat{\gamma}$) we can rewrite (3.32) as

$$\begin{aligned} &\sim \hat{\gamma} \left(\int_{|q_i| >> O(M)} d^4 q \frac{\hat{\gamma}^* [\hat{q}^* \hat{\gamma}] \gamma_- [\hat{q} \hat{\gamma}^*] \gamma_+ [\hat{q}^* \hat{\gamma}]}{[q^2]^3} \right) \frac{\gamma_-}{M^2} \frac{\hat{\gamma}^*}{\hat{k}^*} \\ &\sim \hat{\gamma} \left(\int_{|q_i| >> O(M)} d^4 q \frac{\hat{\gamma}^* \not{q}_\perp (1 - \gamma_5) \gamma_- \not{q}_\perp \gamma_+ \not{q}_\perp}{[q^2]^3} \right) \frac{\gamma_-}{M^2} \frac{\hat{\gamma}^*}{\hat{k}^*} \end{aligned} \quad (3.33)$$

We recognize the integral, within the brackets, of (3.33) as a left-handed transverse propagator contribution to a tensor component of the standard large momentum anomaly integral (apart from the feature that there is no trace of the γ -matrices involved). Therefore, we could anticipate (3.26) directly from the familiar anomaly contribution to a three current vertex $T_{\mu\alpha\beta}(k_1, k_2)$ - the notation is that of Fig. C1. In our case,

$$k_1 = -k_2 = k'_\perp \quad (3.34)$$

and if we consider the decomposition into invariant amplitudes (C.1), (3.26) corresponds to the contribution of the first two terms, which are linear in k_1 and k_2 .

It is very well known that in the three-current vertex the ambiguity of the ultra-violet anomaly contribution is determined by vector current Ward identities that relate the anomaly contribution to infra-red triangle diagram contributions. In our case, we anticipate that there will be a (reggeized) gluon Ward identity which similarly determines the coefficient of the anomaly contribution we have found. We discuss this point further in Section 5. Note, however, that, in the special momentum configuration (3.34), all the other terms in (C.1) vanish - if there are no infra-red divergences to consider. Therefore, in the lowest-order graphs we are discussing, the ultra-violet anomaly contributions we are discussing can not be canceled by the contribution of infra-red transverse momentum regions.

3.11 Reality of the Anomaly Amplitude

It is significant that the anomaly amplitude we have found, although calculated with internal lines on-shell, is real. Indeed there is no evidence, in the amplitude, of either the s - channel or the t - channel intermediate states that are present in the diagram from which it was calculated. At first sight this seems paradoxical since it

would appear that the above analysis of Fig. 3 can be viewed as the calculation of an s - channel discontinuity - via the unitarity cut corresponding to the dashed line in Fig. 10(a).

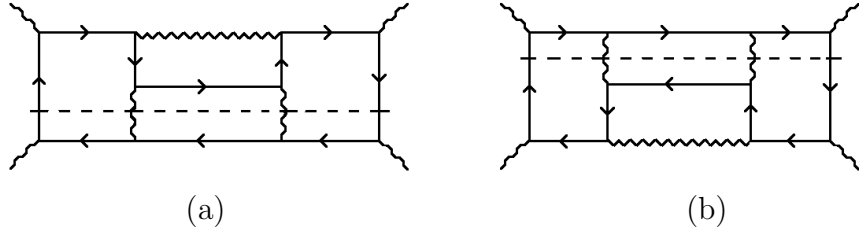


Fig. 10 Unitarity Cuts of (a) the Diagram of Fig. 2 (b) a Related Diagram

The tree amplitude that appears below the cut is integrated with the one loop amplitude that appears above the cut. That the calculation can be related to the evaluation of a discontinuity immediately justifies, in fact, our choice of lines to place on-shell.

That there is ultimately no discontinuity associated with the anomaly is due to a second discontinuity contribution from the unitarity cut of a closely related graph shown in Fig. 10(b). Clearly Fig. 10(b) is so similar to Fig. 10(a) that our analysis carries over directly. In both cases, the intermediate state integration over k_\perp produces an imaginary contribution of $i|S|^{\frac{1}{2}}$. However, the k'_\perp integration, that also gives a factor of $i|S|^{\frac{1}{2}}$, is part of the integration within the loop amplitude.

If we formulate the above analysis as a unitarity calculation then the amplitude on one side of the cut must be complex conjugated. As a result, the loop amplitude will have the opposite sign in the contributions from Figs. 10(a) and 10(b) and since all other parts of the diagrams contribute identically, adding the two will give a factor of

$$(2\pi)^4 \left([i|S|^{\frac{1}{2}}] [i|S|^{\frac{1}{2}}] + [i|S|^{\frac{1}{2}}] [-i|S|^{\frac{1}{2}}] \right) = 0 \quad (3.35)$$

Alternatively, if we calculate the contribution of the two diagrams as that of amplitudes then the loop amplitude will have the same sign in both cases and (3.35) will be replaced by

$$(\pi)^4 \left([i|S|^{\frac{1}{2}}] [i|S|^{\frac{1}{2}}] + [i|S|^{\frac{1}{2}}] [i|S|^{\frac{1}{2}}] \right) = 2\pi^4 S \quad (3.36)$$

which will, indeed, give a real amplitude. The contribution of Fig. 10(b) simply doubles that of Fig. 10(a). The absence of a discontinuity implies that, as we anticipated earlier, there are no additional logarithms accompanying the power enhancement due to the anomaly. The anomaly is a simple pole at $S = \infty$ which results from the combination of the asymptotic pinching of the mass-shell poles of the hatched propagators with the large momentum behavior of the unhatched propagators.

3.12 Another Anomaly Generating Diagram

The diagram of Fig. 10(b) is obtained from that of Fig. 10(a) by simultaneously “twisting” both the left and right-side box diagrams. For much of our discussion (including the addition of extra gluons in the next Section) we will keep the right-side of the diagrams we consider, and therefore the corresponding G_R , fixed and discuss anomaly amplitudes entirely in terms of possible left-side contributions to G_L . In the simple case of the one gluon diagrams that we are presently discussing, the right-side coupling will be that of Fig. 3 (or Fig. 10(a)) and it will be clear that, as in the above discussion, diagrams with the right-side coupling of Fig. 10(b) simply give parallel contributions. However, when we consider infra-red cancelations in the next Section, it will be essential to also consider all contributions to G_R .

Consider, next, the diagram shown in Fig. 11 that is obtained from that of Fig. 3 by twisting the left half of the diagram relative to the right half.

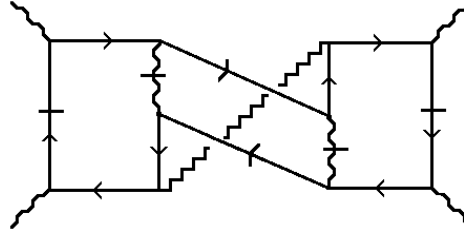


Fig. 11 A Twisted Diagram

By a similar application of the above analysis, which puts on-shell the hatched lines shown in Fig. 11, the transverse momentum diagram of Fig. 1 will again be generated. The G_L shown in Fig. 12(a), obtained from the left part of Fig. 11, contains the effective triangle diagram shown in Fig. 12(b).

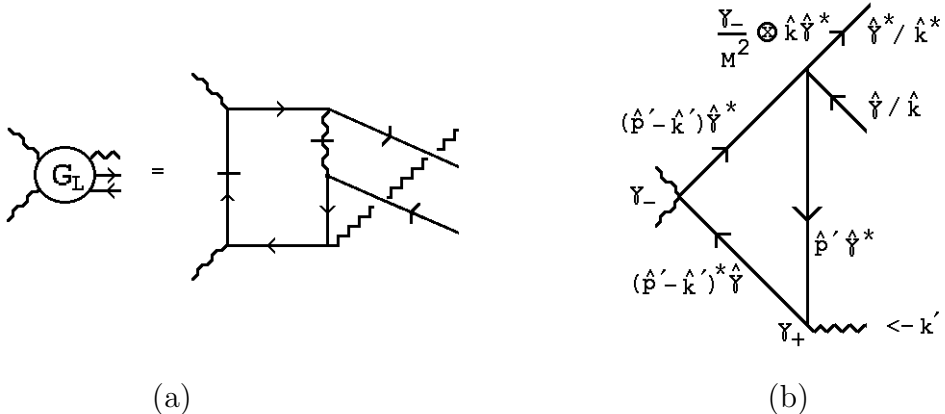


Fig. 12 (a) The G_L Generated by Fig. 11 (b) The Effective Triangle Diagram

A very similar expression to (3.26) will clearly be obtained. The differences in the analysis can be summarized as follows.

- (i) The analogue of (3.12) gives (3.15) but with $\hat{k}[\hat{p}']^* \rightarrow \hat{k}^*\hat{p}'$ which leads to $k_\perp \times p'_\perp \rightarrow -k_\perp \times p'_\perp$ in (3.17) and the following.
- (ii) A second change of sign arises from $k'_\perp \rightarrow -k'_\perp$ in (3.15).

The net result is that an identical anomaly contribution, to that obtained from Fig. 3, is obtained from the diagram of Fig. 11.

The lines placed on-shell, asymptotically, in Fig. 11 do not correspond to a simple cut of the diagram, as was the case for Fig. 3. However, Fig. 11 can also be represented as in Fig. 13(b), i.e. as an exchanged gluon attached to the off-shell lines of the cut amplitude of Fig. 13(a). The exchanged gluon has transverse momentum much less than the off-shell quark or antiquark to which it couples in the large momentum p' and p'' regions which generate the anomaly. Consequently, it does not interfere (kinematically) with either the quark/antiquark scattering process, or the asymptotic placing on-shell of the left side fast quark and the right side antiquark. Therefore, the justification for the choice of lines placed on-shell is closely related to the existence of the asymptotic physical region discontinuity of Fig. 13(a).

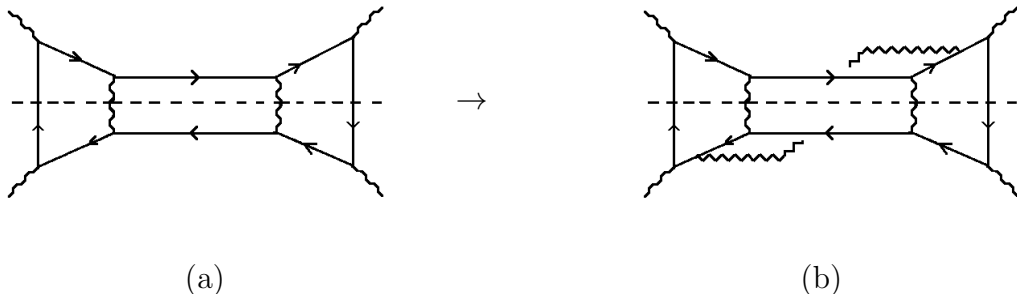


Fig. 13 Addition of an Exchanged Gluon to a Cut Amplitude

The asymptotic pinching of the particle poles that gives the discontinuity in Fig. 13(a), together with the large momentum behavior of the uncut propagators, can be regarded as responsible for the pole at infinite momentum in Fig. 13(b) that corresponds to the anomaly.

A second, essential, point related to the choice of on-shell lines is the following. According to multi-regge theory, the coupling G_L can be evaluated by a double dispersion relation, represented schematically in Fig. 14 - where the cuts represent the discontinuities involved. As a consequence, G_L can be expressed as a sum over dispersion integrals which give amplitudes corresponding to all possible double discontinuities plus, possibly but not necessarily, (generalized) subtraction terms containing

just single discontinuities. The anomaly contributions we have found are, in fact, generalized subtraction terms and the contributions of Fig. 4 and Fig. 12, respectively, correspond to the two single discontinuity terms shown explicitly in Fig. 14.

Fig. 14 Representation of the Double Dispersion Relation for G_L

However, since we are evaluating an amplitude, and not a discontinuity, to have a contribution with on-shell lines corresponding to particular single discontinuities of G_L and G_R , these discontinuities must be present in the asymptotic kinematic region we are considering. In fact, the discontinuity line in Fig. 13(b) can be regarded as representing the combination of the relevant discontinuities of G_L and G_R .

3.13 Possible Cancellation Mechanisms

If we consider just contributions to the transverse momentum diagram of Fig. 1, then Fig. 11 is the only diagram which contributes (via the coupling of Fig. 6(a)) to the same helicity amplitude as Fig. 3 and which generates an appropriate effective triangle diagram, apart from the diagram obtained by similarly twisting Fig. 10(b). We can not twist just the quark-antiquark state since this would reverse the direction of the quark arrow along the fast quark line, requiring a change of the external helicity to obtain a coupling. We conclude, therefore, that the full anomaly contribution to G_L is obtained by adding the two effective triangle diagrams of Fig. 15.

Fig. 15 The Two Effective Triangle Diagrams Generating the Anomaly

Therefore, within the transverse momentum diagram of Fig. 1, the anomaly enhancement does not cancel.

It is natural, however, to expect that there will be further cancellations. As we emphasized in the Introduction, because longitudinal vector meson contributions are involved, it is important to look for all possible cancellation mechanisms that could be associated with an underlying gauge invariance. In particular, because the left-side quark and right-side antiquark are asymptotically on-shell, we must consider whether

asymptotic electroweak Ward identities could lead to the cancelation of the vector meson numerator contributions that are producing the anomaly enhancement.

There are two obvious Ward identity related cancelations that we should consider. First, we consider the tree diagram that appears in the lower half of Fig. 10(a). At finite momentum, if the intermediate state quark and antiquark are strictly on-shell, there will be Ward identities involving this diagram and all other diagrams obtained by attaching the internal vector meson lines at all possible points. Examples of such diagrams, together with the initial diagram, are shown in Fig. 16.

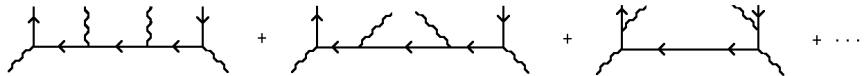


Fig. 16 Tree Diagrams Contributing to an Electroweak Ward Identities

In fact, because the intermediate state quark and antiquark are only asymptotically on-shell, we might expect that only the vector meson numerator components that are parallel to the asymptotic light-cone quark and antiquark momenta must decouple. This decoupling has already appeared in the analysis of sub-section 3.6.

In Appendix D we study in detail the Ward identity cancelations associated with the tree diagrams of Fig. 16. The essential part of the first diagram in Fig. 16 is, indeed, directly canceled by the contribution of the second diagram, which corresponds to the feynman diagram shown in Fig. 17.

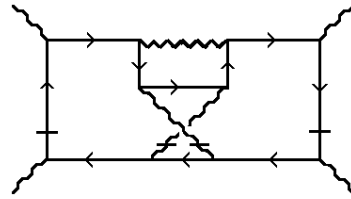


Fig. 17 A Feynman Diagram With a Canceling Anomaly Contribution.

However, the anomaly enhanced amplitude produced by Fig. 17 appears to not be representable as a transverse momentum diagram divergence.

More surprisingly, perhaps, essentially the same anomaly enhanced amplitude then reappears via the contribution of the third diagram in Fig. 16, which corresponds to the feynman diagram shown in Fig. 18. This is a diagram that would normally be neglected because off-shell propagators are carrying large light-cone momenta.

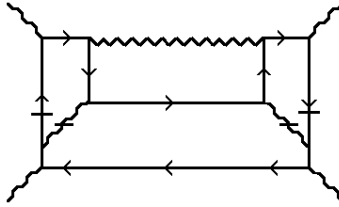


Fig. 18 The Feynman Diagram Corresponding to the Third Tree Diagram in Fig. 16

In a sense, therefore, nothing is gained by implementing the Ward identity cancelations. However, after this implementation it is apparent that the lack of anomaly cancelation is entirely due to the asymptotic nature of the placing on-shell of the quark and antiquark lines. Also, when the Ward identity cancelations are carried out several diagrams are included, in addition to Fig. 18, that would normally be considered non-leading. This makes it clear that there is a general phenomenon of superficially non-leading high-energy behavior contributing to the leading behavior because of large transverse momentum divergences.

There is also a second Ward identity, involving the top part of Fig. 10(a) and other loop diagrams, some of which are shown in Fig. 19, that might be expected to lead to the decoupling of the top $\gamma_- p'_+$ vertex in Fig. 7, together with the corresponding $\gamma_+ p''_-$ right-side vertex. These vertices are crucially important for our analysis.

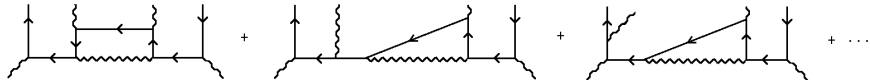


Fig. 19 Loop Diagrams Contributing to Electroweak Ward Identities

However, in this case it is the intervention of the asymptotic anomaly that invalidates the potential asymptotic Ward identities and, self-consistently, prevents the decoupling of the vector meson vertices that are involved.

In conclusion, we can say that there is no cancelation of the transverse momentum coupling effective triangle diagram anomaly by another diagram with a similar anomaly. There may very well be a cancelation outside of the transverse momentum diagram formalism. However, in this paper at least, we will not pursue this possibility any further.

3.14 The Same Helicity Scattering Amplitude

To obtain an anomaly amplitude for the scattering of vector mesons which both have helicity $\lambda = +1$ we include the left side coupling of Fig. 6(b) within a diagram that otherwise is the same as Fig. 3 or Fig. 11. The result is the two

diagrams shown in Fig. 20. When displayed in the first form, it is clear that the only difference between these diagrams and, respectively, Figs. 3 and 11 is that along the left-most vertical line $P_+ \rightarrow -P_+$. Therefore, if we evaluate the diagrams with the sign of P_+ reversed, corresponding to a cross-channel physical region, the appropriate on-shell configurations will be present. The diagrams will be kinematically identical, respectively, to Figs. 3 and 11 and will give identical anomaly contributions, but with $S \rightarrow -S$.

The second form for the diagrams displayed in Fig. 20 is more transparent for discussing symmetry properties of the intermediate state. In particular, in this form, it is clear that Fig. 20(b) can be obtained from Fig. 3 by twisting the quark-antiquark intermediate state (together with the necessary redirection of the quark arrow in the left part of the diagram). Fig. 20(a) can similarly be obtained from Fig. 11.

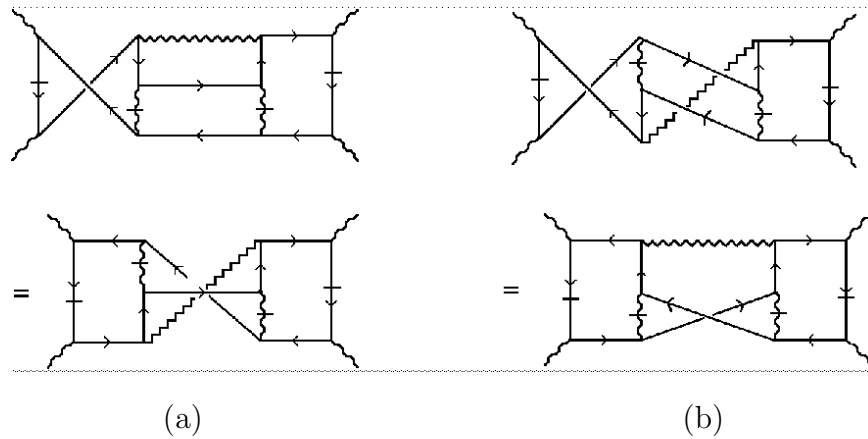


Fig. 20 The Scattering of Same Helicity Vector Mesons

3.15 Cancelation in a Vector Theory

If the vector mesons we are considering had a vector coupling, rather than a left-handed coupling, to quarks, then the diagrams of Fig. 16 would appear also in the opposite sign helicity amplitude but with $(1 + \gamma_5)$ couplings replacing the $(1 - \gamma_5)$ couplings in Fig. 6(b). In this case, after the use of (A.15), the relative minus sign discussed in the previous sub-section (resulting from $S \rightarrow -S$) produces a cancellation between the anomaly contributions from Fig. 3 and Fig. 20(a). Similarly, the contributions from Fig. 11 and Fig. 20(b) cancel. In a vector theory, this cancellation of right and left-handed coupling contributions would persist, even as we add more gluons as discussed in the next Section.

3.16 The Even Signature Amplitude

To form signatured scattering amplitudes we should add to, or subtract from, a particular helicity amplitude the amplitude obtained by a CPT transformation of

one scattering state relative to the other. Therefore, if A_{-+} and A_{++} are the opposite sign and same sign amplitudes we have discussed,

$$A^\pm(P_+, P_-) = A_{-+}(P_+, P_-) \pm A_{++}(-P_+, P_-) \quad (3.37)$$

is an even/odd signature amplitude. This implies that the anomaly amplitudes arising from Fig. 3 and Fig. 20(a) are added in the even signature amplitude and subtracted in the odd signature amplitude (as are, also, the anomaly amplitudes arising from Fig. 11 and Fig. 20(b)). Therefore, the anomaly cancels in the odd signature amplitude and is present only in the even signature amplitude. This will continue to be the case as we add more gluons in the next Section. It is directly related, via a generalization of the discussion of the previous two sub-sections, to the cancelation in a vector theory.

3.17 C and P Properties of the Transverse Momentum State

Since the intermediate state in Fig. 4 is completely transverse (or, equivalently, is a t - channel intermediate state) the T part of the CPT transformation, defining the signature of an amplitude, has no effect on it. Therefore, we should be able to relate signature directly to the CP properties of the transverse momentum state.

The parity transformation reverses the transverse momentum of the gluon and so, because of the coupling (3.26), simply gives a minus sign. Without a color factor, the charge conjugation transformation also gives just a minus sign. Therefore, the gluon component of the intermediate state is even under CP . For quarks the left-handed coupling violates both P and C . As a result, the quark-antiquark intermediate state only has simple transformation properties under the combined CP transformation. Charge conjugation transforms a quark (antiquark) to the corresponding antiquark (quark), with the same helicity (opposite chirality). The parity part of the CP transformation then reverses the helicities. In our case, the quark and antiquark have opposite helicities and so they will be simply interchanged by the CP transformation. Individually, the diagrams we are discussing do not have simple symmetry properties with respect to quark/antiquark interchange. Not surprisingly, however, the full set of anomaly contributions in the even signature amplitude does have such a property.

With the four diagrams, Figs. 3, 11, 20(a) and (b), added in the even signature amplitude, it is clear (using the second display form in Fig. 20) that the left-side coupling is symmetric, diagrammatically, with respect to the interchange of the quark and antiquark. The interchange relates Fig. 3 to Fig. 20(b) and Fig. 11 to Fig. 20(a). In addition to the reversal of the quark line, the contribution of Fig. 20(b) to the even signature amplitude differs kinematically from that of Fig. 3 in two ways that produce canceling sign changes. Firstly, $k_\perp \rightarrow -k_\perp$, and, secondly, the effect in the k'_\perp integration of $P_+ \rightarrow -P_+$ resulting from the definition of the even signature amplitude. Therefore, in this amplitude, the quark/antiquark intermediate state is

even under CP . Since the gluon state is also even under CP , the full transverse momentum state is indeed even under CP , as it should be.

Note that the full even signature amplitude will contain, in addition to the four diagrams of Figs. 3, 11, 20(a) and 20(b), the four related diagrams obtained by substituting the right side of Fig. 10(b) for that of Fig. 10(a). In effect, in this second set of diagrams the twists are made on G_R that are made on G_L in the first set of diagrams. Each set of twists is sufficient to give an intermediate state with the appropriate CP property. As a result, the discussion of each set of four diagrams can be made separately and is directly parallel. In higher orders it will sometimes be necessary to consider both sets of twists together to obtain an intermediate state with the right CP property.

4. COLOR FACTORS AND MORE GLUONS

We begin with a discussion of SU(2) flavor that will, essentially, allow us to ignore it in the following.

4.1 SU(2) Flavor

The SU(2) flavor symmetry will play only a minimal role in our discussion and we will introduce it in a very elementary manner. We consider the exchange of a quark-antiquark $\{I = 1, I_z = 0\}$ state that, in the standard model, would carry the quantum numbers of the π^0 . Identifying W^\pm, W^0 with the $\{I = 1, I_z = \pm, 0\}$ vector mesons and identifying u, d with the $\{I = \frac{1}{2}, I_z = \frac{\pm 1}{2}\}$ quarks, we can add flavor quantum numbers to the discussion of the previous Section by using the vector meson / quark vertices of Fig. 21.

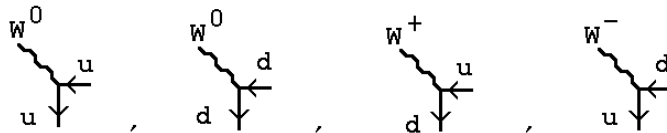


Fig. 21 Vector Meson / Quark Vertices

The flavorless couplings of Fig. 6 are then replaced by the sums of couplings shown in Figs. 22(a) and (b) and the internal vector meson on-shell contributions are replaced by a similar sum.

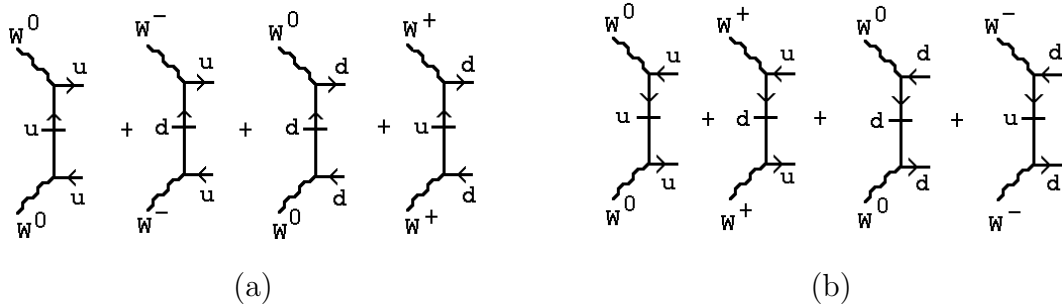


Fig. 22 Couplings with SU(2) Flavor Quantum Numbers

We then add all the diagrams obtained with this set of couplings. The most important feature of these couplings is that they are symmetric with respect to $u \leftrightarrow d$ and that this symmetry is preserved by the internal vector meson exchange interactions. (It is also important for the CP properties of the diagrams we discuss that, in going

from Fig. 22(a) to Fig. 22(b), left-handed quarks and right-handed antiquarks are interchanged, as was the case for Figs. 6(a) and (b).) Consequently, the addition of $SU(2)$ flavor factors will not produce any diagram cancelations and we can leave, as implicit, the replacement of the couplings of Fig. 6 by those of Fig. 22.

4.2 Color Factor Diagrams and the One Gluon Color Factor

$SU(3)$ color factors will also be relatively simple. In all the diagrams we discuss, there will be only one quark loop. There is no external color and so color is introduced into the quark loop only by the couplings to the internal gluons. Also, for the diagrams we consider, gluons will appear only as part of the exchanged transverse momentum state and will be attached within the corresponding G_L and G_R transverse momentum couplings. As a result, we can use a simple notation to describe color factors. We represent the quark loop as a rectangle, and attach gluons only to the vertical lines. The attachment of gluons to the left-side vertical line represents the order of attachment to the quark loop within the left-side transverse momentum coupling G_L , while the right-side vertical line similarly represents the order of attachment within G_R . For each gluon there is a color matrix λ_i at each attachment point. The full color factor is the trace of the product of the λ - matrices taken around the loop, and then summed over $i = 1, \dots, 8$ for each gluon. The notation is illustrated for various numbers of exchanged gluons in Fig. 23.

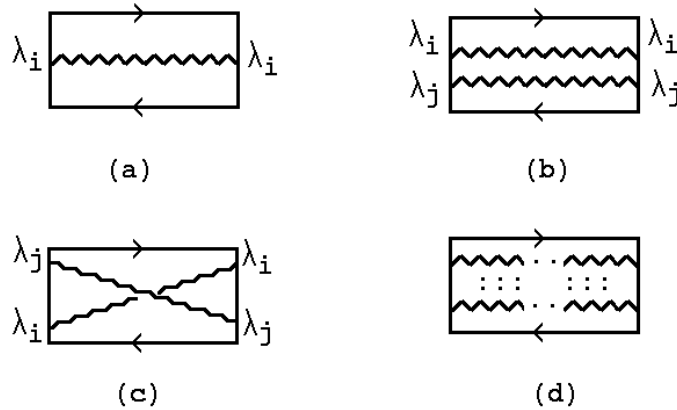


Fig. 23 Color Factor Diagrams

All of the diagrams discussed in the previous Section contain just one gluon and have the same color factor. This is represented by Fig. 23(a) and is simply

$$\sum_i \text{Tr}\{\lambda_i^2\} \quad (4.1)$$

Since all diagrams have the same color factor (and flavor factor) all of the discussion in the previous Section is essentially unchanged, apart from the discussion of charge conjugation, which now has to include color charge conjugation.

For a general gluon field with color matrix M_{ab} , color charge conjugation is defined as

$$M_{ab} \rightarrow [-M_{ab}]^T = -M_{ba} \quad (4.2)$$

For the hermitian color matrix vertices λ_i

$$[-\lambda_i]^T = -[\lambda_i]^* \quad (4.3)$$

where $[]^*$ denotes complex conjugation. Therefore, in addition to the charge conjugation minus sign discussed in the last section, the coupling of the gluon to the quark line (within G_L , say) is complex conjugated. Correspondingly, for the quark-antiquark pair, in addition to the charge conjugation discussed in the previous Section, quark/antiquark interchange gives

$$[\lambda_i]^* \rightarrow [\lambda_i] \quad (4.4)$$

in (4.3). Since the parity transformation is unchanged, the full gluon plus quark/antiquark transverse momentum state remains even under CP when color charge conjugation is included.

4.3 The Addition of a Soft Gluon

Next, we look for feynman diagrams that contain two gluons and that also, potentially, contain the anomaly enhancement. We will assume that only one gluon is involved in the transverse momentum divergence and will consider two possibilities for the scale of the transverse momentum carried by the second gluon. It can either be “soft”, i.e. it carries a very small momentum k'' , with

$$|k''_\perp| \ll M \ll |k_\perp|, |k'_\perp| \leftrightarrow \text{“soft”} \quad (4.5)$$

or “finite”, i.e.

$$|k''_\perp| \sim M \ll |k_\perp|, |k'_\perp| \leftrightarrow \text{“finite”} \quad (4.6)$$

As we will see, in some diagrams soft gluon exchange is possible, in addition to the anomaly generation, while in others only finite gluon exchange is possible. In both cases, the second gluon will provide an important color factor. A soft gluon, however, will also produce an infra-red divergence. Since the full transverse momentum state carries zero color, such divergences must cancel. This will help us to locate other diagrams generating the anomaly.

We consider the “soft” gluon case first and look for diagrams that contribute to the transverse momentum diagram of Fig. 24 which, as discussed further in Appendix B, would again be expected to contribute (formally) only at next-to-next-to-leading log. (Note that, when the anomaly is not present, this diagram again, potentially, includes a logarithmic transverse momentum divergence generating an additional energy logarithm.)

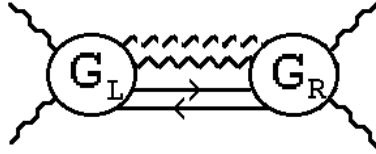


Fig. 24 The Two Gluon Transverse Momentum Diagram - the Broken Line Denotes a Soft Gluon

We begin with the addition of a soft gluon to the diagram of Fig. 3. The anomaly will appear in the same manner as before if, in the high-energy limit, an effective triangle diagram is generated as in Fig. 4, but with the additional gluon attached, via a point coupling, to one of the three vertices of the diagram. The required local coupling could appear, in principle, if k'' can be directed through an adjacent quark line which can be put on-shell by the k''_\perp integration. If this line carries (predominantly) a large light-cone momentum then, in analogy with (3.3), the integration will produce couplings that are independent of k''_\perp . In Figs. 25(a), (b), and (c) we show how the extra gluon could be added to Figs. 6, 7, and 8, respectively, with the final γ - matrices remaining the same as in Fig. 9.

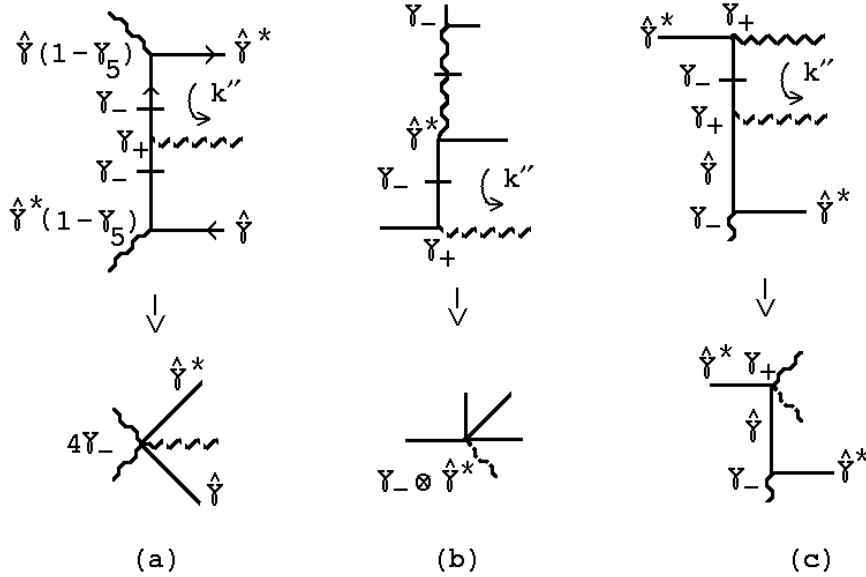


Fig. 25 Adding a Gluon to the Vertices of (a) Fig. 6 , (b) Fig. 7 , and (c) Fig. 8

In Fig. 25(c) the soft and hard gluon can be interchanged, whereas in Figs. 25(a) and (b) there is no ambiguity as to where the soft gluon has to be attached, if the γ - matrix structure is to remain the same.

For Fig. 25(a) we can, essentially, apply (3.3) directly. For the couplings of Figs. 25(b) and (c) there is, however, a problem if the extra gluon is soft and so carries

only very small transverse momentum. In these cases, the propagator that has to be placed on-shell by the k''_- - integration is adjacent to an off-shell propagator that, in the anomaly configuration, is carrying very large transverse momentum (p'_\perp). In this case the mass-shell condition is

$$k''_- \sim \frac{(p'_\perp + k''_\perp)^2}{p'_+} \sim \frac{\epsilon M \sqrt{S}}{\epsilon \sqrt{S}} \sim M \quad (4.7)$$

which can not be satisfied with $k''_- \ll |k''_\perp| \ll M$. Therefore, if the vertex for the extra gluon is of the form of Fig. 25(b) or (c), in both the G_L and G_R couplings, then it can not carry $|k''_\perp|^2 \ll M^2$.

Later, we will discuss potential contributions from vertices of the form of Fig. 25(b) and (c) when k'' is “finite”, i.e. $|k''_\perp|^2 \sim M^2$. For the moment, we consider only the vertex of Fig. 25(a). Generation of the corresponding triangle diagram is shown in Fig. 26

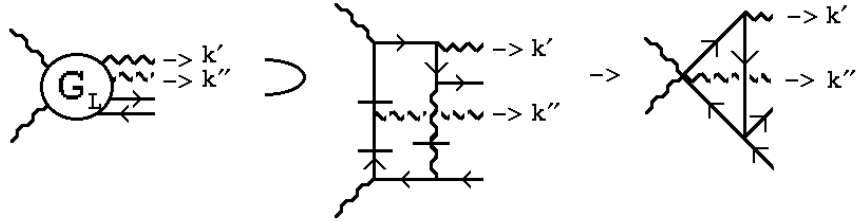


Fig. 26 A Two Gluon Effective Triangle Diagram

and the full feynman diagram, with the extra gluon attached in the same manner to both sides of Fig. 3, is shown in Fig. 27.

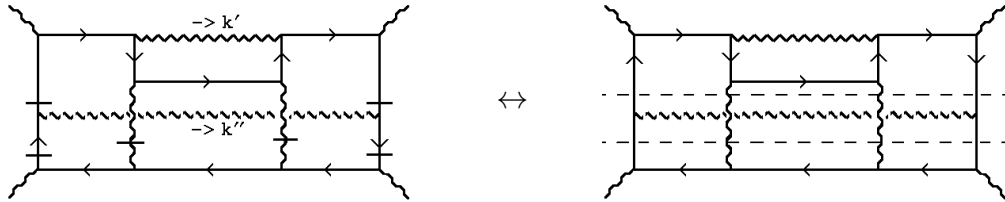


Fig. 27 A Two Gluon Feynman Diagram With Two Cuts

As illustrated, the lines put on-shell correspond to making a double cut of the diagram. This corresponds to double discontinuity contributions to the G_L and G_R couplings. (These contributions are again generalized subtractions in that the full dispersion relations for G_L and G_R contain triple discontinuities.)

4.4 The Two Gluon Anomaly Amplitude

If k''_\perp is much smaller than any other transverse momentum in the diagram of Fig. 23, the only significant k''_\perp dependence will be in the k'' propagator. Hence, the k''_\perp integration can be factored out from the remaining integrations and, before the inclusion of any color factor, the diagram of Fig. 23 gives, via the reduction of Fig. 25(a) and Fig. 26, a high-energy anomaly enhanced amplitude of the form

$$\begin{aligned}
& \int^{|k''_\perp| < M} \frac{d^2 k''_\perp}{k''_\perp^2} \int \frac{d^2 k'_\perp}{k'_\perp^2} \int d^2 k_\perp \left(\frac{k_\perp \times k'_\perp}{M^2} \right)^2 \frac{\text{Tr}\{\gamma_- \hat{\gamma}^* \gamma_+ \hat{\gamma}\}}{\hat{k} \hat{k}^*} \\
& \sim \left(\int^{|k'_\perp| < M} \frac{d^2 k''_\perp}{k''_\perp^2} \right) \int \frac{d^2 k'_\perp d^2 k_\perp}{k'_\perp^2 k_\perp^2} \left(\frac{k_2 k'_3 - k_3 k'_2}{M^2} \right)^2 \\
& \sim \left(\int^{|k''_\perp| < M} \frac{d^2 k''_\perp}{k''_\perp^2} \right) \int^{O(MS^{\frac{1}{2}})} \frac{d(k'_\perp^2)}{M^2} \int^{O(MS^{\frac{1}{2}})} \frac{d(k_\perp^2)}{M^2} \\
& \sim S / M^2
\end{aligned} \tag{4.8}$$

We can similarly add a soft gluon to each of the one gluon diagrams discussed in the last Section and generate a high energy amplitude of the same form. There is, however, clearly a divergence at $|k''_\perp|^2 = 0$ that we must discuss. First, however, we discuss the relevant color factors.

4.5 Two Gluon Color Factors

There are two possible color factors for the transverse momentum diagram of Fig. 24. They are shown in Figs. 23(b) and (c) and have the form

$$(b) \sum_{i,j} \text{Tr}\{\lambda_j \lambda_i \lambda_i \lambda_j\} \quad (c) \sum_{i,j} \text{Tr}\{\lambda_i \lambda_j \lambda_i \lambda_j\} \tag{4.9}$$

We discuss these two factors in a manner that will generalize when further gluons are added. The essential formula we need is

$$\lambda_i \lambda_j = \frac{2}{3} \delta_{ij} + \sum_k (i f_{ijk} + d_{ijk}) \lambda_k \tag{4.10}$$

which, since f_{ijk} is antisymmetric and d_{ijk} is symmetric, implies that

$$\lambda_j \lambda_i + \lambda_i \lambda_j = \frac{4}{3} \delta_{ij} + 2 \sum_k d_{ijk} \lambda_k \tag{4.11}$$

and

$$\lambda_j \lambda_i - \lambda_i \lambda_j = -2i \sum_k f_{ijk} \lambda_k \tag{4.12}$$

Therefore, the sum of the two color factors (4.9) is given by

$$\begin{aligned}
\sum_{i,j} Tr\{\lambda_j\lambda_i\lambda_i\lambda_j + \lambda_i\lambda_j\lambda_i\lambda_j\} &= \sum_{i,j} Tr\{[\frac{4}{3}\delta_{ij} + 2\sum_k d_{ijk}\lambda_k]\lambda_i\lambda_j\} \\
&= \sum_{i,j} Tr\{[\frac{4}{3}\delta_{ij} + 2\sum_k d_{ijk}\lambda_k] [\frac{2}{3}\delta_{ij} + \sum_l d_{ijl}\lambda_l]\} \\
&= \sum_{i,j} [\frac{8}{9}\delta_{ij} + \frac{4}{3}\sum_k d_{ijk}^2] = 20\frac{4}{9}
\end{aligned} \tag{4.13}$$

and the difference of the two gives

$$\begin{aligned}
\sum_{i,j} Tr\{\lambda_j\lambda_i\lambda_i\lambda_j - \lambda_i\lambda_j\lambda_i\lambda_j\} &= \sum_{i,j,k,l} Tr\{[-2i f_{ijk}\lambda_k]\lambda_i\lambda_j\} \\
&= \sum_{i,j,k} Tr\{[2i f_{jik}\lambda_k] [i f_{ijl}\lambda_l]\} \\
&= \sum_{i,j,k} \frac{4}{3} f_{ijk}^2 = 12
\end{aligned} \tag{4.14}$$

Both (4.13) and (4.14) are expressed as a sum of squares of color factors where each individual term corresponds to a particular color for the gluon intermediate state. The states that contribute can be found by writing the left-side color factor as a sum over distinct intermediate states, as is effectively done in (4.11) and (4.12). The full color factor can then be written, relying on the orthogonality of the intermediate states, as a sum of squares of the left-side factors. The quark-antiquark intermediate state can only carry zero or octet color. Correspondingly, since the total color of the intermediate state is zero, the gluon sums must also contribute either zero or octet color. This will continue to be the case when more gluons are present in the transverse momentum state. For the two gluon case, as illustrated in Fig. 28,

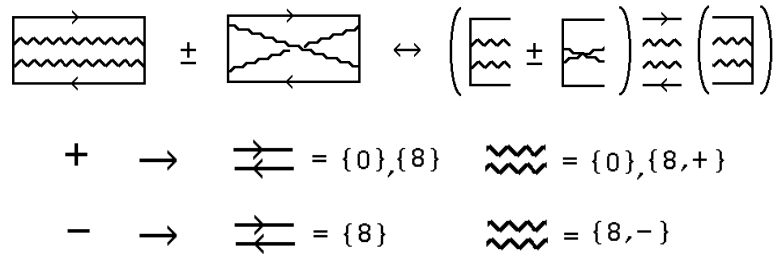


Fig. 28 Color Breakdown of the Intermediate State

in the symmetric color factor (4.13) the gluon sums give zero and octet color contributions, which both have even color parity. In the antisymmetric factor (4.14) only the color octet with odd color parity contributes.

4.6 The Color Factor for the Anomaly

Consider again the effective triangle diagram of Fig. 22. (As in the last Section, we will initially discuss only the various anomaly contributions to G_L , with G_R kept fixed.) Comparing with the diagrams of Fig. 4 and Fig. 12(a), the twisted triangle diagram that should give an anomaly contribution to add to that of Fig. 26 is that shown in Fig. 29(a) and the corresponding full diagram is that of Fig. 29(b).

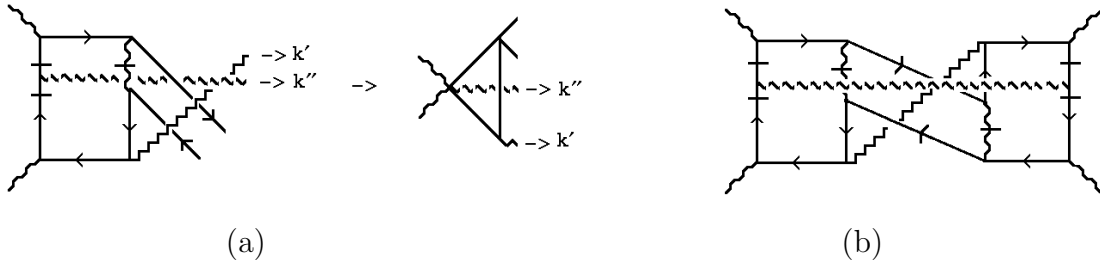


Fig. 29 (a) A Twisted Effective Diagram (b) The Full Twisted Diagram

As illustrated in Fig. 30 and in analogy with Fig. 13, Fig. 29(b) can be obtained by adding an exchanged gluon to the two cut amplitude of Fig. 30(a).

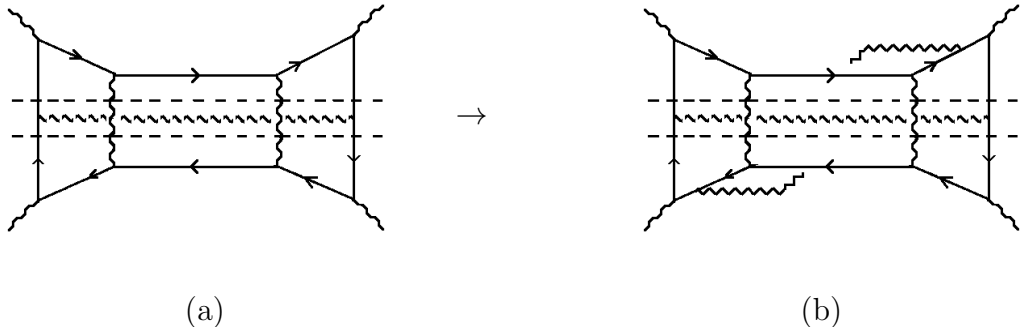


Fig. 30 Addition of an Exchanged Gluon to a Two Cut Amplitude

Again, in the anomaly region, with $|k'_\perp|^2 \ll |p'_\perp|^2, |p''_\perp|^2$, the exchanged gluon does not interfere, significantly, with the kinematics of taking the double discontinuity of Fig. 30(a). It is also clear from Fig. 30, that the on-shell lines of Fig. 29(b) correspond to physical double discontinuities of the G_L and G_R .

If we consider the order of λ matrix multiplication (following the quark arrow) we see that it is reversed for the two gluons in Fig. 29(a) compared to those in Fig. 26. As a result, if we add the two diagrams the anomaly is multiplied by the sum of the two color factors (4.13). As we have discussed, in this case there are separate contributions corresponding to whether the quark-antiquark pair is in a color octet or a color zero state.

4.7 Signature and Color Charge Parity

To form signatured amplitudes we consider, with the diagrams of Fig. 27 and Fig. 29(b), the corresponding diagrams for same helicity vector scattering. These are shown in Figs. 31(a) and (b), respectively. With flavor included, the left-hand couplings in these diagrams should be replaced by the full, flavor symmetric, couplings of Fig. 22(b), while the right-hand couplings should continue to be the analogue of Fig. 22(a). As in Fig. 18, we display the diagrams in two different ways, each of which will be simpler for particular arguments.

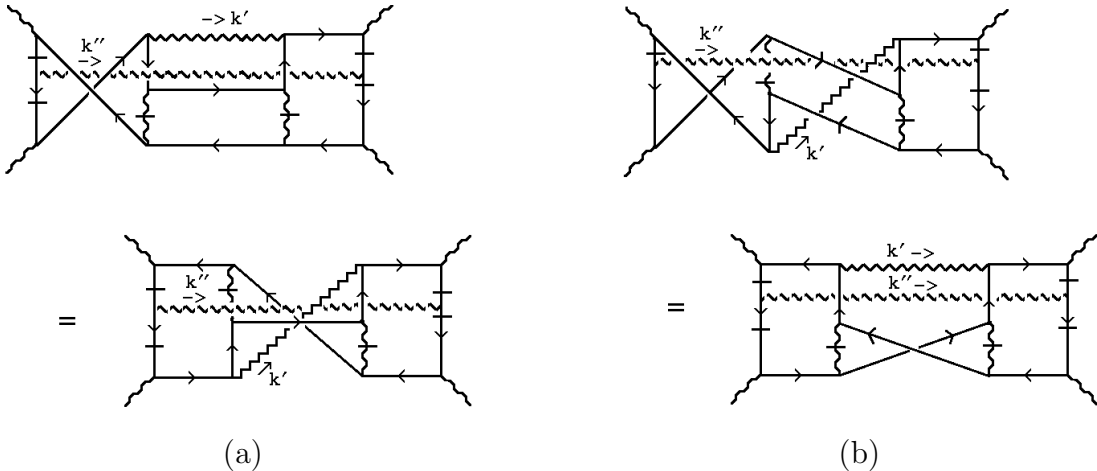


Fig. 31 Same Helicity Scattering Diagrams With One Soft Gluon

To discuss signature we focus on the first forms displayed. Comparing with our discussion of the diagrams of Fig. 20, we note that Figs. 31(a) and (b) again differ, kinematically, from Fig. 27 and Fig. 29(b) (respectively) only in that $P_+ \rightarrow -P_+$ along the left-most vertical line. Therefore, if we evaluate the diagrams of Fig. 31 in the cross-channel physical region - with the sign of P_+ reversed, they will be kinematically identical, respectively, to Figs. 27 and 29(b) and will give identical anomaly contributions, but with $S \rightarrow -S$. Therefore, these diagrams have anomaly contributions with the opposite sign to those of Figs. 26 and 29(b) and in a vector theory would provide a cancelation. In the present case, since the color factors are the same, the anomaly contributions of the two diagrams of Fig. 31 add to those of Figs. 27 and 29(b) in the even signature amplitude and produce a cancelation in the odd signature amplitude.

As in our discussion of the one gluon diagrams, we can also obtain the signature from the CP symmetry properties of the intermediate transverse momentum state. We consider, first, properties of the gluon component. Since the gluons have only QCD vertices, they can have simple transformation properties under C and P separately.

Applying color charge conjugation to (4.11) gives

$$\begin{aligned} [\lambda_j \lambda_i + \lambda_i \lambda_j] &\rightarrow (-1)^2 [\lambda_j^* \lambda_i^* + \lambda_i^* \lambda_j^*] \\ &= [\lambda_j \lambda_i + \lambda_i \lambda_j]^* = \frac{2}{3} \delta_{ij} + \sum_k d_{ijk} [\lambda_k]^* \end{aligned} \quad (4.15)$$

The parity transformation reverses the transverse momentum of the gluons and so, because of the coupling (3.26) for the large transverse momentum gluon, again gives a minus sign. Therefore, the full effect of the CP transformation of the gluon component of the intermediate state is given by

$$\frac{2}{3} \delta_{ij} + \sum_k d_{ijk} [\lambda_k] \rightarrow -\frac{2}{3} \delta_{ij} - \sum_k d_{ijk} [\lambda_k]^* \quad (4.16)$$

Comparing (4.15) and (4.16) with (4.11) we observe that the color zero two gluon state carries negative CP and is separately even under C and odd under P . It therefore has “normal” color charge parity (equal to the number of gluons in the state) but has “anomalous” negative parity, producing an “anomalous” negative signature. The color parity of the octet gluon state is also well-defined if we ignore $[\lambda_k] \rightarrow [\lambda_k]^*$ (which is, of course, compensated for by the quark/antiquark interchange discussed below) and is similarly even.

To discuss the CP transformation of the quark/antiquark pair we compare with our discussion in sub-section 3.15 and note, first, that the left-side coupling of Fig. 31(b) can be obtained, diagrammatically, from that of Fig. 27 by quark/antiquark interchange. The left-side coupling of Fig. 31(a) can similarly be obtained from that of Fig. 29(b). In the even signature amplitude we must evaluate the diagrams of Fig. 31 with $P_+ \rightarrow -P_+$ compared to the other diagrams. Therefore, quark/antiquark interchange now gives three kinematic changes of sign

$$\begin{aligned} (i) \quad & k_\perp \rightarrow -k_\perp \\ (ii) \quad & k'_- \rightarrow -k'_- \quad \text{from} \quad P_+ \rightarrow -P_+ \\ (iii) \quad & k''_- \rightarrow -k''_- \quad \text{from} \quad P_+ \rightarrow -P_+ \end{aligned} \quad (4.17)$$

When all four diagrams are added the amplitude is, kinematically, antisymmetric under quark/antiquark interchange. As a result, when the quark/antiquark pair has color zero it is, straightforwardly, negative under CP . Combined with the negative CP of the color zero two gluon state this gives no change under the full CP transformation, as is necessary to obtain an even signature amplitude.

When octet color is involved, the color effect of interchanging the quark-antiquark pair will, as we already noted above, again be $[\lambda_h] \rightarrow [\lambda_h]^*$. Therefore,

with the negative sign coming from the kinematic interchange, the complete CP transformation on the quark-antiquark pair again combines with the octet part of (4.16) to produce an overall positive CP result for the full two gluon quark-antiquark state.

4.8 Infra-Red Cancelations

Since (4.8) contains an infra-red divergence (at $k''_\perp^2 \sim 0$), and there is no external color, there must be other anomaly contributions that cancel this divergence. Before discussing the possible diagrams that could be involved, it will be useful to first discuss the lower limit on the k''_\perp^2 integration in Fig. 27.

The momentum flow through the two lines that are put on-shell by the k'_- and k''_- integrations is shown in Fig. 32.

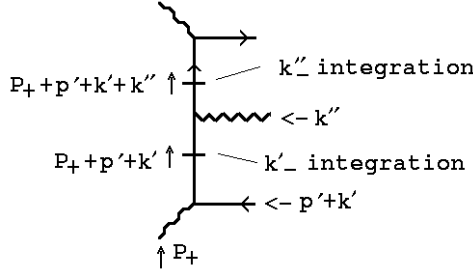


Fig. 32 Momentum Flow for the k'_- and k''_- Integrations

Since k'_\perp is large and k'' is small, all the large momenta flow through both lines. Therefore, the large momenta are significantly constrained by the k' mass-shell condition before the k'' mass-shell condition is imposed. If we, temporarily, introduce a quark mass m then the k'_- mass-shell condition is $(P_+ + p' + k')^2 = m^2$ and, with this constraint, the mass-shell condition for k''_- becomes

$$k''_- \sim \frac{-2k''_\perp(p' + k')_\perp + m^2}{P_+} \quad (4.18)$$

$$\underset{k''_\perp \rightarrow 0}{\sim} \frac{m^2}{S^{\frac{1}{2}}}$$

If k''_+ is similarly constrained, and (to justify the reduction to a transverse momentum diagram) we require $k''_\perp^2 \gtrsim |k''_- k''_+|$, the lower limit for the k''_\perp - integration is

$$|k''_\perp|^2 \sim \frac{m^4}{S} \quad (4.19)$$

and so an infra-red divergence appears at $|k''_\perp|^2 = 0$, as $S \rightarrow \infty$, of the form

$$\int_{|k''_\perp|^2 \sim \frac{m^4}{S}} \frac{d^2 k''_\perp}{k''_\perp^2} \sim \ln S - \ln m^4 \quad (4.20)$$

As we discuss briefly in the next Section, we expect the cancelation of the infra-red divergence (4.20) to be a consequence of a Ward identity that results from attaching the soft gluon at every possible point around the effective triangle diagram. Consider, therefore, the attachment of the soft gluon, in G_L , according to the other possibilities illustrated in Fig. 25. With the attachment shown in Fig. 25(b) we obtain the full diagrams shown in Fig. 33.

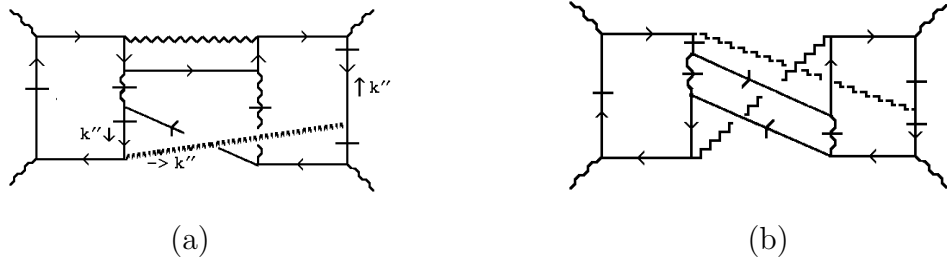


Fig. 33 Diagrams Obtained with the Soft Gluon Attachment of Fig. 25(b)

The mass-shell condition now has the form (4.7) and so, if the lower limit for the k'_+ integration still has the form (4.18), requiring $|k'_\perp|^2 > k'_+ k'_-$ gives the lower limit

$$|k'_\perp|^2 \sim \frac{m^2 M}{S^{\frac{1}{2}}} \quad (4.21)$$

Therefore, if the diagrams of Fig. 33 give anomaly contributions they will have, as a factor, an infra-red divergence of the form

$$\int_{|k''_\perp|^2 \sim m^2 M / S^{\frac{1}{2}}} \frac{d^2 k''_\perp}{k''_\perp^2} \sim \frac{1}{2} \ln S - \ln m^2 - \ln M \quad (4.22)$$

If, instead, one attachment of the soft gluon is that of Fig. 25(c) rather than that of Fig. 25(b), as we have just discussed, there will clearly be a similar infra-red divergence.

There is, however, a major reason why the diagrams of Fig. 33, ultimately, do not give an anomaly contribution. Because of the location of the soft gluon attachment, the sign change (iii) in (4.17) will not be present when $P_+ \rightarrow -P_+$ in the diagrams appropriately related to those of Fig. 33 in the same sign helicity amplitude.

As a result, in the even signature anomaly amplitude, the quark-antiquark intermediate state must be positive under CP . Alternatively, if we add all the diagrams related to those of Fig. 33 that give all possible contributions to each G_R , we will obtain G_R couplings to the quark-antiquark intermediate state that have negative CP . Therefore, when all diagrams related to those of Fig. 33 are added in the even signature amplitude, the resulting G_L requires positive CP for the quark-antiquark state, while the G_R requires negative CP . Consequently, if there is an anomaly contribution from any of the diagrams, it must cancel in the sum.

This last problem similarly applies to all diagrams in which one soft gluon attachment is as in Fig. 25(c) while the other attachment is that of Fig. 25(a). As we will shortly discuss there will, nevertheless, be important anomaly contributions from diagrams in which the attachments of the second gluon, in both G_L and G_R , are either of the form of Fig. 25(b) or Fig. 25(c). In this case, however, the second gluon necessarily has “finite” transverse momentum and so can not produce an infra-red divergence.

To look further for a divergence that could cancel that due to Fig. 27, we must consider whether there are any new kinematic configurations, generating the anomaly and involving a soft gluon, that can not be viewed as a soft gluon accompanying the one gluon enhancement diagrams. In fact, if we are considering the attachment of the soft gluon at every possible point around the effective triangle diagram, there is one possibility that we have not yet included or discussed. This is to interchange the momenta of the two gluons involved in Fig. 26. In Fig. 34 we show the full diagram obtained from Fig. 27 by interchanging k' and k'' in one side of the diagram relative to the other.

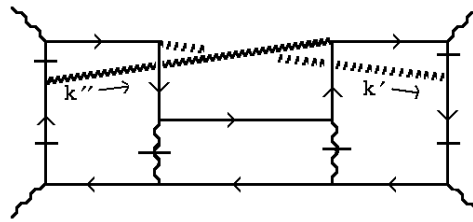


Fig. 34 The Diagrams Obtained by Interchanging k' and k'' in Fig. 27

The soft gluon is again indicated by a broken line. (Note that Fig. 34 is symmetric with respect to k' and k'' , if we interchange the roles of G_L and G_R .)

If we interchange k' and k'' in Fig. 26, then the large transverse momentum flows into the triangle diagram at the left-most vertex while the single gluon vertex carries only small transverse momentum. This does indeed give an anomaly contribution. This contribution has, however, some different properties compared to those we have so far discussed. In Fig. 35 we compare the large momentum route for k'

with the possible routes for k'' , around the same triangle.

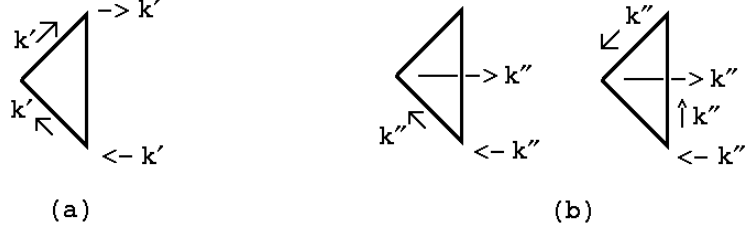


Fig. 35 (a) Momentum Route for k'_\perp (b) Possible Routes for k''_\perp

We observe, first, that while the route for k' large was determined by the particles we wished to put on shell, there are two possible routes if k''_\perp is large. As illustrated, it could flow through either one or two quark propagators. From (3.21) and (3.22), we see that the anomaly contribution is obtained from an expansion in powers of $|k''_\perp/p'_\perp|$ (in which the first term does not contribute). Consequently, if k''_\perp appears in only one propagator, rather than two, the anomaly contribution will be reduced by a factor of 1/2 (in the even signature amplitude where both chiralities are added for each propagator). The sign will also be opposite. This is the normal ambiguity of the ultra-violet anomaly, that occurs because of the choice of momentum routing, which we expect to be determined by a Ward identity.

If k' is small, the k'' mass-shell condition does not constrain the large transverse momentum (p'_\perp) involved in the k'_\perp mass-shell condition. As a result, the k'_\perp mass-shell condition gives a constraint similar to (4.7), i.e.

$$k'_\perp \sim \frac{p'^2}{P_+} \sim \frac{\epsilon M S^{\frac{1}{2}}}{S^{\frac{1}{2}}} \sim \epsilon M \quad (4.23)$$

Since the k'_+ integration in G_R has the lower limit (4.18), we will again obtain an infra-red divergence of the form of (4.22). In this case, however, since there is a gluon attached to both the left and right side quark lines, there is no CP conflict. Also, from Fig. 36, it is clear that neither gluon interferes with the kinematics of the quark sub-amplitude, which remains such that the vector meson lines can consistently be placed on-shell.

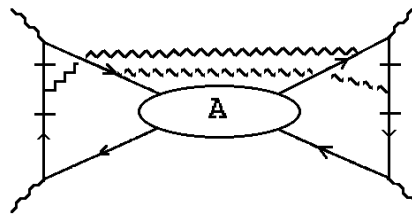


Fig. 36 Two Gluons Accompanying the Quark Sub-Amplitude

In fact, if the anomaly has the sign and magnitude obtained from the second routing of Fig. 35(b) (which is the “normal” routing), there will be a cancellation with the divergence obtained from Fig. 27 when the diagram of Fig. 34 is added and the two contributions, from k'' large and k' small, and k' large and k'' small, are combined.

At this point we note that k' is the total momentum flowing in at a “vector” vertex of an effective triangle diagram with an anomaly. In this case, as we discuss in the next Section (and illustrate for the usual triangle anomaly in Appendix C), we expect that the appropriate Ward identity, which would determine which routing in Fig. 35(b) is correct, will involve both the large internal momentum region of the triangle diagram that generates the anomaly and a small internal momentum region that produces a very different kinematic form, containing the “anomaly pole”. The discussion of the anomaly pole and pion wee gluon couplings that we have given in [8] should, essentially, carry over to an infra-red analysis of effective triangle vertices that would be the analogue of the ultra-violet analysis presented in this paper. This analysis must be carried out before we can establish, in detail, how the (reggeon) Ward identities are satisfied, and that infra-red divergences are indeed eliminated when the diagram of Fig. 34(a) is added to that of Fig. 27.

4.9 Anomalous Color Parity Gluons

In the final form of two gluon anomaly contributions that we consider the second gluon transverse momentum k''_\perp is neither very small, nor grows with S . It is “finite”, i.e. $O(M^2)$. In the diagrams we consider, the above discussion implies that the kinematics of the anomaly prevent the second gluon from carrying very small transverse momentum. In particular, we consider diagrams of the form shown in Fig. 37, in which the second gluon attachment is the same in both G_L and G_R , and has the form of either Fig. 25(b) or Fig. 25(c).

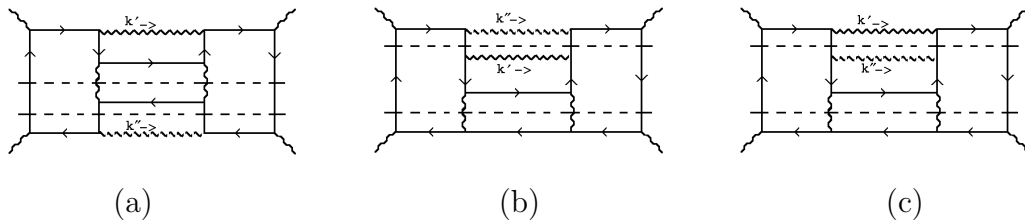


Fig. 37 Gluon Attachments (a) - as in Fig. 25(b), or (b) and (c) - as in Fig. 25(c)

The broken gluon line in these diagrams now indicates finite transverse momentum and the lines put on-shell correspond, as illustrated, to two cuts through each diagram. The combination of particle poles giving these two discontinuities, together with the off-shell loop, that occurs either at the top, in the middle, or at the bottom, in the three diagrams, is now responsible for the anomaly. (As usual, a closely related set of diagrams is obtained by twisting simultaneously both the G_L and the G_R in each

of these diagrams. For Fig. 37(a) the same diagram is actually obtained, but the kinematic regions for the two gluons are interchanged.)

To form signatured amplitudes, as before, we consider the same helicity scattering amplitudes shown in Fig. 38.

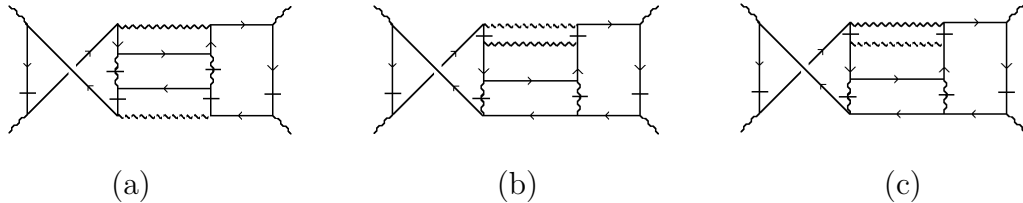


Fig. 38 Same Helicity Diagrams Related to the Diagrams of Fig. 37

Again we can argue that these diagrams are related to those of Fig. 37 by $P_+ \rightarrow -P_+$ and so the same anomaly amplitude is obtained, but with $S \rightarrow -S$. Therefore, these diagrams give anomaly contributions that add to those of Fig. 37 in the even signature amplitude. However, as in our discussion of the diagrams of Fig. 23, because the finite gluon is not attached to the fast left side quark, the sign change (iii) in (4.17) will not be present when $P_+ \rightarrow -P_+$ in the diagrams of Fig. 38. Consequently, the G_L coupling obtained by adding the diagrams of Fig. 38 to those of Fig. 37, requires even CP for the quark-antiquark intermediate state. When the corresponding diagrams are added, this argument will similarly apply to G_R . As a result, the quark-antiquark state is necessarily positive under CP . This can be consistent with even signature for the complete intermediate state only if the two gluon state is also even under CP . This can, in turn, only be the case if the two gluon state carries antisymmetric octet color and so has, “anomalous”, odd color charge parity (not equal to the number of gluons).

In the two gluon anomaly contributions that we have discussed in previous sub-sections, the two gluon state has carried normal color charge parity because the addition of twisted diagrams gave the symmetric color factor. We must consider, therefore, whether there are also “twisted diagrams” related to those of Fig. 37 which cancel the antisymmetric part of the color factor.

Twisted diagrams related to the diagrams of Fig. 37 are shown in Fig. 39. For Figs. 39(a) and (b), the color factor is indeed reversed compared, relatively, to Figs. 37(a) and (b). Also, it is clear that, in Figs. 39(a) and (b), the appropriate (hatched) lines can be consistently placed on shell. (This is not true for other diagrams that could, potentially, be related, by twisting, to either of Fig. 37(a) or (b).) Therefore, as before, adding the diagrams of Figs. 39(a) and (b) to those of Figs. 37(a) and (b) gives the symmetric color factor and so, because the quark-antiquark state has even CP , the anomaly contribution must cancel in the sums of these diagrams.

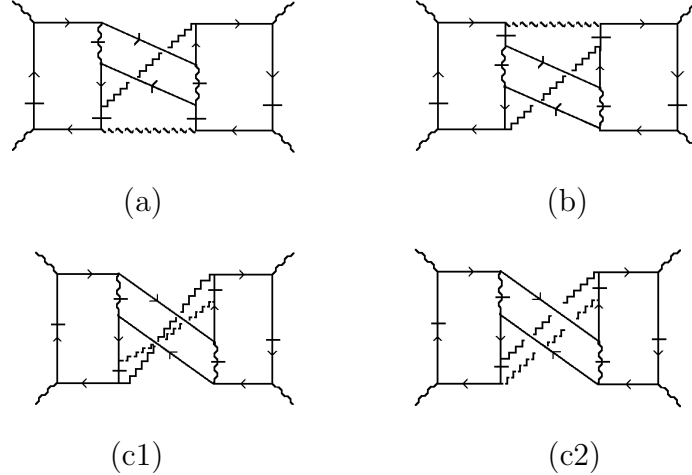


Fig. 39 Diagrams Related to the Diagrams of Fig. 33 by Twisting

Both Fig. 39(c1) and Fig. 39(c2) can be regarded as twisted relative to Fig. 37(c). For Fig. 39(c1) the color factor is reversed compared to Fig. 37(c), but the hatched lines clearly can not be consistently placed on-shell in the physical region. For Fig. 39(c2) it seems probable that the hatched lines can be placed on-shell consistently, even though the necessary cuts would cross. The issue is irrelevant, however, since Fig. 39(c2) has the same color factor as Fig. 37(c). In fact, there is no twisted diagram corresponding to Fig. 37(c) which has a reversed color factor and in which all the necessary hatched lines can be consistently placed on-shell.

Since we can regard the color factor for Fig. 37(c) as the sum of the symmetric and antisymmetric factors, the antisymmetric, odd color parity, component will be selected for the anomaly contribution from this diagram (and it's same helicity counterpart). Similarly for Fig. 39(c2), if it contributes. Together with the contribution of corresponding diagrams obtained by twisting both G_L and G_R , these will be the only anomaly contribution from diagrams in which the second gluon carries “finite” transverse momentum. In all cases, the second gluon is attached as in Fig. 25(c), and not as in Fig. 25(b). The finite gluon contributions have the important property that the two gluon state carries “anomalous color parity”. This is significant because, as we emphasized in the Introduction, reggeized gluon exchanges that appear in vector theory perturbative calculations[1]-[7] carry normal color parity. The appearance of anomalous color parity gluon states is, therefore, a direct consequence of the presence of the anomaly.

4.10 General Multigluon Color Factors

Before considering more complicated multigluon configurations we give a general discussion of multigluon color factors which generalizes the previously discussion of two gluon color factors.

We note first that we can obtain (4.11) and (4.12) from (4.10) by a more general argument than just the symmetry and antisymmetry of the d and f tensors. Consider a product of λ - matrices

$$P_{1n} = \prod_{j=1}^n \lambda_{i_j} \quad (4.24)$$

together with the product taken in the reverse order

$$P_{n1} = \prod_{j=n}^1 \lambda_{i_j} \quad (4.25)$$

Using (4.10) extensively we can write

$$P_{1n} = A_{1n} + \sum_k B_{1nk} \lambda_k \quad (4.26)$$

where A_{1n} multiplies the unit matrix and both $A_{1n} = A_{i_1, i_2, \dots, i_n}$ and $B_{1n} = B_{i_1, i_2, \dots, i_n, k}$ contain combinations of f and d tensors. Similarly, we can write

$$P_{n1} = A_{n1} + \sum_k B_{n1k} \lambda_k \quad (4.27)$$

(4.26) and (4.27) decompose P_{1n} and P_{n1} , respectively, into a sum of color singlet and color octet contributions.

It follows from the hermiticity of the λ_i that

$$(P_{n1})^T = \prod_{j=n}^1 (\lambda_{i_j})^T = \prod_{j=n}^1 (\lambda_{i_j})^* = (P_{1n})^* \quad (4.28)$$

where $(\)^T$ denotes transposition and $(\)^*$ denotes complex conjugation. Equivalently,

$$P_{n1} = ((P_{1n})^T)^* \quad (4.29)$$

As a result

$$A_{n1} = A_{1n}^*, \quad B_{n1k} = B_{1nk}^* \quad (4.30)$$

or, equivalently,

$$\begin{aligned} P_{1n} + P_{n1} &= 2 \operatorname{Re}(A_{1n}) + 2 \operatorname{Re}(B_{1nk}) \lambda_k \\ P_{1n} - P_{n1} &= 2i \operatorname{Im}(A_{1n}) + 2i \operatorname{Im}(B_{1nk}) \lambda_k \end{aligned} \quad (4.31)$$

which gives ((4.11) and (4.12), as a very simple case.

Since the f and d tensors are both real, it follows from (4.10) that a factor of i is always accompanied by an f tensor. Therefore, the real and imaginary parts of both A_{1n} and B_{1n} contain, respectively, even and odd numbers of f tensors. If we then consider

$$Tr\{\Sigma_{i_1,i_2,\dots,i_n}(P_{1n} \pm P_{n1})(P_{1n})\} \quad (4.32)$$

the distinct color of A_{1n} and B_{1n} and the distinct symmetry properties of the real and imaginary coefficients implies that

$$Tr\{\Sigma_{i_1,i_2,\dots,i_n}(P_{1n} + P_{n1})(P_{1n})\} = 2 \Sigma_{i_1,i_2,\dots,i_n}([Re(A_{1n})]^2 + [Re(B_{1n})]^2) \quad (4.33)$$

which is a sum of the squares of color factors for color zero and color octet states which contain an even number of f - tensors and so describe normal color parity gluon states. Similarly,

$$Tr\{\Sigma_{i_1,i_2,\dots,i_n}(P_{1n} - P_{n1})(P_{1n})\} = -2 \Sigma_{i_1,i_2,\dots,i_n}([Im(A_{1n})]^2 + [Im(B_{1n})]^2) \quad (4.34)$$

which is a similar sum of squares of color factors which, because they contain an odd number of f tensors, describe gluon states with anomalous color charge parity.

In the two gluon states that we have so far considered, all color factors apart from the first term in (4.34) have appeared. This term corresponds to a color zero anomalous color parity multigluon configuration. It will appear in the three gluon diagrams that we discuss next. We continue to confine our discussion to a single large transverse momentum gluon and consider only multiple soft or finite gluon contributions that do not involve any factors of lnS . (In general, we anticipate that higher order logarithms lead to the separate reggeization of each of the transverse momentum gluons in the diagrams we study.)

4.11 Two Soft Gluons

We begin with two soft gluons and consider diagrams that contribute to the transverse momentum diagram of Fig. 40.

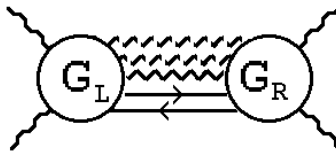


Fig. 40 A Transverse Momentum Diagram With Two Soft Gluons

We will straightforwardly obtain an anomaly enhanced amplitude, as before, from diagrams in which two soft gluons are attached to the external effective point vertices, as illustrated in Fig. 41.

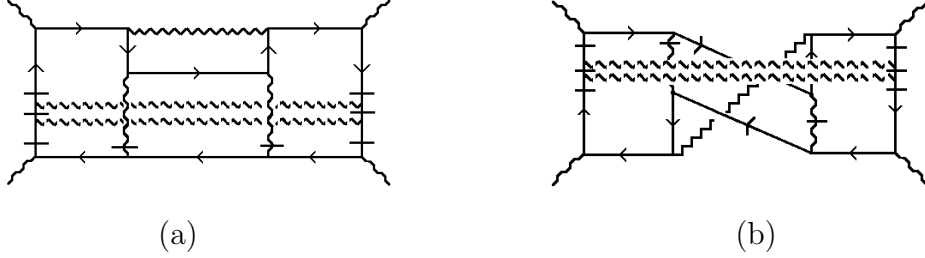


Fig. 41 Diagrams With Two Soft Gluons

Because all the large momenta pass through both soft gluon attachments and are constrained by the k'_- integration, the infra-red scale is the same for both and is $m^2/S^{\frac{1}{2}}$, as in (4.18) and (4.19). Infra-red cancelations can, presumably, be discussed in the same manner as in our discussion of one soft gluon diagrams. The twisted diagram of Fig. 41(b) again reverses the color matrix multiplication of Fig. 41(b) and so the sum of the two diagrams gives a color factor of the form of (4.33), corresponding to normal color parity for the complete three gluon transverse state

To check that the anomaly amplitude obtained is even signature we note that the anomaly diagrams in the same sign helicity amplitude will again be related to the opposite sign diagrams by $P_+ \rightarrow -P_+$. For example, the diagram of Fig. 37(a) will be related to a same sign helicity amplitude diagram as illustrated in Fig. 42

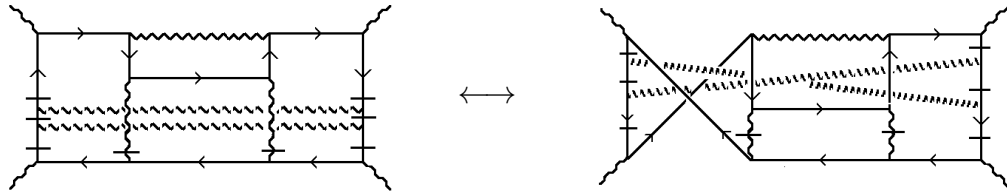


Fig. 42 Related Diagrams in Different Helicity Amplitudes

Since the color factors are the same, these amplitudes are again related by $S \rightarrow -S$ and will add in the even signature amplitude (and would cancel in a vector theory).

As before, the full gluon state will have negative parity because of the single large transverse momentum gluon. Combined with the negative (normal) color parity this implies that the three gluon state is even under CP . Repeating the discussion of the quark/antiquark state that we gave for the one soft gluon amplitudes we find that there is an additional change of sign from $P_+ \rightarrow -P_+$ that results from the additional soft gluon. As a result, quark/antiquark interchange gives no kinematic change of sign and the color charge parity transformation simply gives $\lambda_h \rightarrow \lambda_h^*$. Consequently, the full quark/antiquark/multigluon intermediate state is even under CP , as required for even signature. (We should note, however, that although the color zero three gluon

state has normal color charge parity, it is “anomalous” in that it has negative parity, giving an “anomalous” positive signature.)

4.12 Color Zero Anomalous Color Parity

Consider, next, adding a soft gluon to the diagrams of Figs. 37(c) and 38(c), in which there is already one finite transverse momentum gluon present. If the soft gluon is attached to the left and right side quark lines, the resulting opposite sign and same sign helicity diagrams are shown, respectively, in Figs. 43(a) and (b).

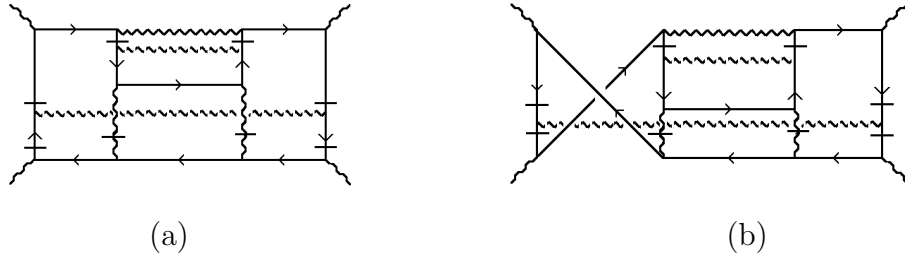


Fig. 43 Anomalous Color Parity Diagrams With One Soft and One Finite Gluon

The color factor for both diagrams is the same, i.e.

$$\sum_{i,j,k} \text{Tr}\{\lambda_k \lambda_j \lambda_i \lambda_i \lambda_j \lambda_k\} \quad (4.35)$$

If we pick out the color zero intermediate state then the color factors on the left and right side of the diagrams must separately factor into traces. Therefore, we can write

$$\begin{aligned} \sum_{i,j,k} \text{Tr}\{\lambda_k \lambda_j \lambda_i \lambda_i \lambda_j \lambda_k\} &\sim \sum_{i,j,k} \text{Tr}\{\lambda_j \lambda_i \lambda_k\} \text{Tr}\{\lambda_i \lambda_j \lambda_k\} + \dots \\ &\sim \sum_{i,j,k} f_{ijk}^2 + \dots \end{aligned} \quad (4.36)$$

where the term we have shown explicitly is the color zero, anomalous (even) color parity, term.

Because, the diagrams of Fig. 43 contain one less gluon attached to the fast quark lines than the diagrams of Fig. 42, the quark-antiquark component of the transverse state, in the even signature amplitude, will be odd under CP . Therefore, to obtain even signature overall the gluon component must also be odd under CP , implying that is even under color charge conjugation. Consequently, the anomalous color parity term, shown explicitly in (4.36), is selected for the color zero component of the combination of the diagrams of Fig. 43 in the even signature amplitude.

4.13 Multigluons

Clearly we could generalise the foregoing discussion to a variety of multigluon configurations involving combinations of soft and finite gluons, with effective vertices of the form illustrated in Fig. 44.

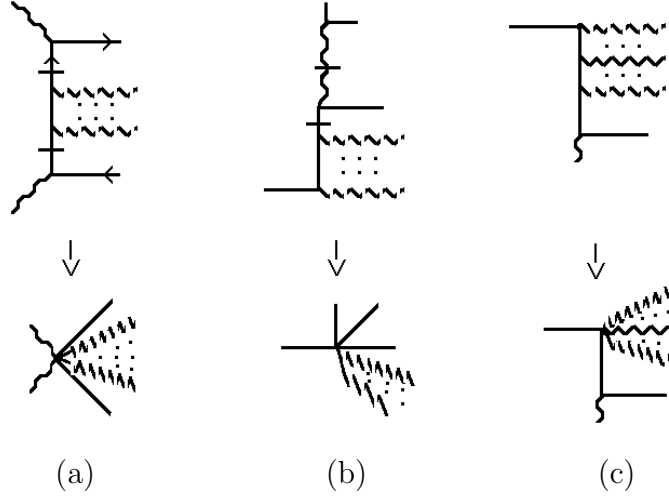


Fig. 44 Multi-gluon Effective Vertices

However, having established the coupling of color zero anomalous color parity gluons, we have all the general properties that we require for the discussion of the next Section.

Since a large transverse momentum gluon can give a scaling contribution of the form

$$\sim \int_{(k''_\perp)^2 \sim \sqrt{s}} \frac{d^2 k''_\perp}{(k''_\perp)^2} \quad (4.37)$$

it is also possible for additional large transverse momentum gluons to participate in the enhancement effect. Potentially, this could be an elaborate phenomenon involving, presumably, the reggeization of both quarks and gluons and, in higher orders, scaling properties of reggeized gluon interactions, as well as the evolution of α_s . However, since we will argue, in the next Section, that large transverse momentum anomaly contributions are unphysical, there seems little point in exploring the issue any further. In part, we discuss the analogous infra-red phenomenon in the next Section.

5. REGGEON WARD IDENTITIES, CUT-OFFS, AND INFRA-RED DIVERGENCES

Our calculations in the previous Sections have demonstrated that the anomaly enhanced diagrams, some of which contain anomalous gluons, provide the dominant contribution in the exchange channel we have considered. However, as we remarked in the Introduction, we believe that the power enhancement involved should not be present in physical amplitudes. Assuming that there is no perturbative cancelation, via some mechanism that has yet to be elucidated, then obtaining “physical” amplitudes without the enhancement is, *a priori*, a challenging problem.

In this Section we will briefly outline how we anticipate the desired physical amplitudes can be obtained. The essential point will be that the contribution of the anomaly diagrams is very different if we take the regge limit before or after the removal of an ultra-violet transverse momentum cut-off. This cut-off introduces infra-red divergences and if it is removed only at a very late stage, as we will propose, then the result obtained will also depend on whether all orders sums are performed before or after it is removed and on how, and at what stage, infra-red cut-offs (in the form of gluon and quark masses) are removed. This ambiguity is the essence of the anomaly and it would not be surprising if there is a unique procedure that is necessary to obtain the right “physical” answer.

As we have already noted, both in the Introduction and in the previous Section, a study of the infra-red anomaly contributions of the diagrams we have considered, that matches the present study of ultra-violet contributions, will be necessary before any detailed arguments can be carried through. To fully elucidate infra-red anomaly contributions it will surely be necessary to abandon the restriction to forward kinematics and transverse polarizations that has greatly simplified the foregoing discussion. Nevertheless, based on our experience with hadron scattering amplitudes[8], we believe that a complete procedure for obtaining physical amplitudes can be developed utilizing the following, briefly summarized, properties. Our hope is that since the present starting point is much simpler than the hadronic problem, the analysis will be correspondingly more straightforward.

5.1 Ward Identity Consequences and a Transverse Momentum Cut-Off

Gauge invariance implies that a general amplitude $\langle A_\mu(q) \dots \rangle$ with all (external) lines on shell except for one gluon that carries four momentum q satisfies the simple Ward identity

$$q_\mu \langle A_\mu(q) \dots \rangle = 0 \quad (5.1)$$

This identity usually follows[12], at a given order in perturbation theory, only after the zero momentum gluon has been attached to the remainder of the diagram at all

possible points. It is well-known that this identity, in turn, implies that the gluon amplitude vanishes at zero four momentum. Also, from analogous Ward identities[12], a similar result holds when more than one gluon carries vanishing four momentum. (If the gauge symmetry is spontaneously-broken then, of course, the Ward identities corresponding to (5.1), such as the “electroweak Ward identities” referred to in subsection **3.13**, have additional mass terms which prevent the infra-red vanishing of amplitudes.)

The vanishing of a loop amplitude when external momenta are small compared to (“finite”) internal momenta also implies, generally, a suppression of internal momenta that are large compared to, finite, external momenta. If, however, there is an external axial current producing an anomaly contribution in a loop, then the situation is different. In this case, as we briefly review in Appendix C, in addition to the well-known anomalous Ward identity [13] for the axial current, vector Ward identities require a cancelation between separate contributions, with different kinematic structure, from large and small internal momentum regions. In particular, the large momentum anomaly contribution (C.5) cancels with an infra-red term that, in special momentum configurations (and only when the quarks are massless), reduces to a simple pole in the axial vector channel. This is the “anomaly pole” that can, in the right circumstances, be interpreted as a Goldstone boson pole, signaling chiral symmetry breaking. In addition to the discussion in Appendix C, a detailed analysis of the anomaly pole, and the internal momentum region generating it, can be found in[8].

In general, the above properties of gluon amplitudes, as functions of four-dimensional momenta, transfer directly[14] to corresponding properties for the multi-gluon (multi-reggeon) transverse momentum couplings that we discuss in this paper, as functions of transverse momenta. The linear vanishing when transverse momenta are scaled to zero is sufficient to eliminate infra-red divergences in the transverse momentum diagrams that we consider. If there is an anomaly in a transverse momentum coupling then, as we already noted in our discussion of infra-red cancelations in **4.8**, there will be large/small internal momentum cancelations in the associated transverse momentum (reggeon) Ward identities that parallel the cancelations that take place in the four-dimensional Ward identities. We expect that infra-red divergences will be avoided, in part, by cancelation of the ultraviolet anomaly contributions we have found with infra-red “anomaly pole” contributions. In fact, the coefficient of the anomaly in a transverse momentum coupling (which we did not determine) should be fixed by this cancelation.

If we impose a transverse momentum cut-off in all internal loop integrals of the diagrams we consider, this cut-off will be present in all transverse momentum diagram integrals and also within the loop integrals giving the external couplings. A cut-off in the transverse momentum diagram integrals is gauge invariant. A priori,

however, in the external couplings such a cut-off is not gauge invariant. Therefore, if we take the regge limit with a transverse momentum cut-off imposed, it will be a serious question whether gauge invariance is restored by removing the cut-off after the limit. For the present we note only that in [8] we argued that anomaly pole contributions to infra-red divergent amplitudes are gauge invariant.

In the infra-red region, we anticipate that there will be effective triangle diagram contributions to G_L and G_R couplings in which small transverse momentum gluons couple at all three vertices, as illustrated in Fig. 45.

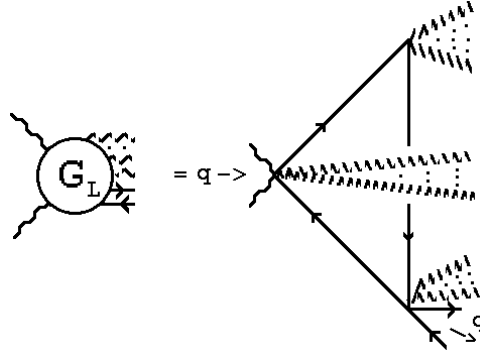


Fig. 45 An Infra-Red Effective Triangle Diagram

Based on the analysis of the previous Section, both normal and anomalous color parity multigluon states should couple. With a transverse momentum cut-off imposed we expect that, when the total gluon transverse momentum vanishes the corresponding Ward identity will fail and there will be a non-zero coupling involving (when the quarks are massless) the anomaly pole. As a consequence, in transverse momentum diagrams of the form of Fig. 40 (with all gluons soft) there will be a logarithmic infra-red divergence of the form

$$\int^{\lambda_\perp} \frac{dQ^2}{Q^2} \quad (5.2)$$

where Q is the sum of all gluon transverse momenta.

A priori, the anomaly pole can appear in both G_L and G_R . However, at $t = 0$, where the pole should appear, a finite light-like momentum can be exchanged which can be parallel to either P_+ or P_- . We suspect that this light-cone momentum determines whether the pole appears via G_L or G_R . Clearly, a detailed study, of the kinematics/polarizations and kinematic forms associated with the appearance of the anomaly pole will be needed to be sure that, in the full amplitude, there is a simple pole with the appropriate residue to be associated with a pion.

5.2 Transverse Momentum Infra-red Divergences

Since the divergence (5.2) is not removed by external couplings (with a trans-

verse cut-off), we must consider the effect of (all orders) interactions amongst the gluons. In the lowest-order diagrams we expect the divergence to be present for both normal and anomalous color parity gluon states. There may also be additional divergent transverse momentum configurations. However, as we now describe, when we sum all infra-red divergences to all orders we expect that (5.2) is the only divergence that survives, and then only for anomalous gluons.

We can summarize the general nature of gluon infra-red transverse momentum divergences and the role of a transverse momentum cut-off, very briefly, as follows. An expanded version of this summary can be found in [8]. For reasons that will become apparent in the next sub-section we specifically discuss the case of $SU(2)$ color, although all the properties we describe remain the same for higher gauge groups.

The self-interactions of an N gluon transverse momentum state T_N are described by dimensionless ‘‘kernels’’ $K_N^I(\dots, k_i, \dots, k_j', \dots)$, where I denotes $SU(2)$ color. (Each iteration of a kernel produces an additional factor of $\ln S$, or $(J-1)^{-1}$ in the J -plane, which we will not show explicitly.) When the t -channel color is non-zero the infra-red divergences related to regularization do not cancel and

$$\int \prod_{i=1}^N \frac{d^2 k_i}{k_i^2} K_N^I(\dots, k_i, \dots, k_j', \dots) \rightarrow \infty, \quad Q^2, I \neq 0 \quad (Q = \Sigma_i k_i) \quad (5.3)$$

As a result, the sum of all diagrams in any colored channel exponentiates to zero as illustrated in Fig. 46.

$$\sum \left(G_N^I \right) \left(T_N \right) \left(K_N^I \right) \dots \left(T_N \right) \left(K_N^I \right) \rightarrow 0 \quad I \neq 0$$

Fig. 46 Iteration of a Gluon Kernel K_N .

G_N^I is an external coupling analogous to the G_L and G_R appearing in the previous Sections.

When $I = 0$ and $Q^2 \neq 0$, there is a cancellation of divergences in the K_N^0 . (This is the infra-red finiteness property which is extensively exploited in BFKL applications.) At the leading-log level, infra-red finiteness leads directly to conformal scale invariance. When renormalization effects are introduced, scale invariance is lost in the ultra-violet region. Scale invariance properties may still be present in the infra-red region (in particular, they will be present if there is an infra-red fixed point for the gauge coupling). In this case, the kernels K_N^0 will scale canonically as $Q^2 \rightarrow 0$ so

that, with a transverse momentum cut-off λ_\perp ,

$$\int_{|k_i|^2, |k'_j|^2 < \lambda_\perp} \prod_i \frac{d^2 k_i}{k_i^2} \prod_j \frac{d^2 k'_j}{k'_j^2} K_N^0(k_1, \dots, k_N, k'_1, \dots, k'_N) \sim \int^{\lambda_\perp} \frac{dQ^2}{Q^2} \quad (5.4)$$

The presence of the cut-off ensures that this divergence is unambiguously isolated from ultra-violet divergences with which it might mix.

This is the same divergence as (5.2), which appears in the lowest-order diagrams. The kernels K_N^0 have Ward identity zeroes which result in the special property that iteration of any K_N^0 does not increase the degree of divergence. Instead, there is a distinct contribution from each T_N and the residue of the divergence can be written in a factorized form, as illustrated in Fig. 47.

$$\left(\sum \left[\begin{array}{c} G_N^0 \\ \hline \end{array} \right] \text{---} \text{---} T_N \text{---} \text{---} \left[\begin{array}{c} K_N^0 \\ \hline \end{array} \right] \text{---} \text{---} T_N \text{---} \text{---} \left[\begin{array}{c} K_N^0 \\ \hline \end{array} \right] \text{---} \text{---} \right) \text{---} \text{---} T_N \text{---} \text{---} \left(\sum \text{---} \text{---} T_N \text{---} \text{---} \left[\begin{array}{c} K_N^0 \\ \hline \end{array} \right] \text{---} \text{---} T_N \text{---} \text{---} \left[\begin{array}{c} K_N^0 \\ \hline \end{array} \right] \text{---} \text{---} G_N^0 \right)$$

Fig. 47 Isolation of the Divergence Associated with T_N .

If there is no Ward identity zero in the external couplings G_N^0 , (5.4) is a potential source of a simple infra-red divergence at $Q^2 = 0$.

Similar properties to the above hold for the interactions of gluons with quarks. Crucially, however, there is no kernel describing a transverse momentum interaction between a quark/antiquark pair and an anomalous gluon state. This is because anomalous gluons couple only through an anomaly and anomalies can not occur within the two-dimensional kinematics that the kernels describe.

5.3 SU(2) Color and Reggeon Field Theory

If we consider all the diagrams discussed in previous Sections, generalized to include arbitrary numbers of gluons, and add both interactions amongst the gluons and between the quark-antiquark pair, we arrive at the set of transverse momentum diagrams shown in Fig. 48.

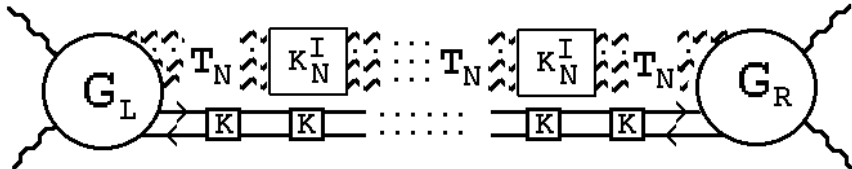


Fig. 48 A Class Of Transverse Momentum Diagrams

If the gluons are anomalous and carry zero color, they will have no interaction with the quark-antiquark pair and the divergence (5.4) will occur when the transverse momentum of all gluons is scaled to zero. As we discussed above, the anomaly pole should appear in the coefficient of this divergence, presumably, with the right kinematic structure to be interpreted as a pion pole. All other similar diagrams, in which either the color is non-zero or the gluons are not anomalous will be exponentiated to zero by interactions that iterate the divergence. However, since the cut-off has still to be removed and it is unclear how to handle the infra-red divergence, the result is still far from a sensible amplitude.

To obtain a more sensible result, we have to use a more sophisticated treatment of the infra-red divergences. In particular, we initially take the $SU(3)$ gauge symmetry of QCD to be partially broken to $SU(2)$. We could motivate this by noting, first, that the structure of the anomaly diagrams is much simpler. Only odd numbers of anomalous gluons can carry color zero (because of the absence of the d -tensor). An overall logarithmic infra-red divergence will still occur, as we have discussed in the previous sub-section, because of the unbroken $SU(2)$ gauge symmetry. However, some gluons (that are massive and outside the $SU(2)$ subgroup) will interact with the quark-antiquark pair. Also, we might hope to eliminate the divergence by averaging over the direction of the $SU(2)$ subgroup within $SU(3)$, as the transverse momentum cut-off is removed.

With these last observations in mind, it is easy to appreciate why Reggeon Field Theory (RFT) should be applied to the problem. In formulating the study of the QCD pomeron using RFT we have argued[7, 10, 14], that we should start from the reggeon diagrams (or, equivalently, transverse momentum diagrams) in which the gauge symmetry is completely broken. With a transverse momentum cut-off, the gauge symmetry can first be restored to $SU(2)$ and the resulting reggeon diagrams can be described by Super-Critical Pomeron RFT - provided all infra-red divergences can be absorbed into a “pomeron condensate”.

For our present problem we anticipate applying RFT as follows. With $SU(3)$ color broken to $SU(2)$, we consider all diagrams of the form illustrated in Fig. 49. In these diagrams, anomalous gluons (within an $SU(2)$ subgroup) accompany a quark-antiquark pair that is interacting with massive, reggeized, gluons. The massive gluons are outside the $SU(2)$ subgroup and carry non-zero transverse momentum.

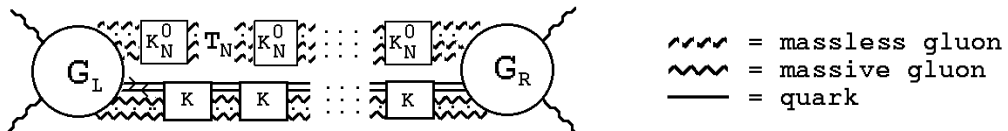


Fig. 49 General Diagrams With a Divergence

This set should map completely on to Super-Critical RFT diagrams containing both pomerons (with the pomeron being a massive reggeized gluon plus anomalous SU(2) gluons) and a reggeized Goldstone boson pion. In this mapping, the physical significance of the logarithmic infra-red divergence would be clear. It would be identified as responsible for the appearance of a pomeron condensate.

The restoration of SU(3) gauge symmetry would be described by the Critical Pomeron[15] interacting with a regge pole pion and (with the appropriate quark sector present[7]-[8]) the transverse momentum cut-off can be removed as part of the critical phenomenon. Also, as part of the critical phenomenon, the SU(2) direction of the pomeron condensate would be randomized within SU(3) and disappear. In effect, the infra-red divergence, producing the condensate, would be eliminated by averaging over the direction of the SU(2) subgroup within SU(3).

For hadron scattering it was important[8] that the pomeron condensate could be related to an anomalous gluon component of the scattering states. This was necessary, firstly, because the γ_5 anomaly coupling of the pion to the pomeron is produced by a product of three orthogonal γ matices. To obtain this product, it was essential to have anomalous gluon components in both the scattering pion and the exchanged pomeron. As we have seen, in electroweak scattering this requirement is absent because the vector mesons have elementary γ_5 couplings, which allow the anomalous gluons to appear in just the exchanged channel. However, the gluon components of the scattering states also seemed to be important for the higher-order pomeron interactions needed to obtain the Critical Pomeron. It may be, therefore, that RFT can only be consistently applied to the analysis of infra-red divergences if the scattering vector mesons are also “hadronic”. That is, if they also have an anomalous gluon component, as they would have if they aquire their mass by absorbing Goldstone bosons resulting from QCD chiral symmetry breaking - with the quarks being color sextet quarks. The presence of the sextet quarks would produce[7]-[8] an infra-red fixed-point (in the massless quark theory) that would guarantee the infra-red scaling of gluon kernels producing (5.4) and would also produce the “quark saturation” of QCD that we have argued is needed to obtain the Critical Pomeron with no transverse momentum cut-off. Perhaps, all these features are needed to obtain a self-consistent description of the regge limit for left-handed, massive, electroweak vector bosons.

6. CONCLUSIONS

We have demonstrated that the triangle anomaly appears in the couplings of transverse momentum diagrams that describe the high-energy scattering of $W^{\pm,0}$ vector mesons. When the full amplitudes are directly evaluated, without any special cut-off procedure, the anomaly produces an enhancement, by a power of the energy, that threatens the unitarity of the theory.

The most well-known consequence of a large momentum triangle anomaly is the famous anomalous Ward identity for axial currents[13]. Less emphasized is the feature that, in the presence of the anomaly, vector Ward identities are satisfied by a subtle cancelation between the contributions of large and small internal momentum regions. In the vector meson scattering we have discussed, an effective current component with an anomaly appears and it is the less emphasized feature that plays a crucial role. Even though there are no anomaly-related cancelations between large and small internal momenta in the finite momentum Ward identities, in a left-handed gauge theory, it appears that the regge limit enhances large transverse momentum regions such that there are cancelations of this kind in the transverse momentum (reggeon) Ward identities. There is then an “anomaly problem” in the sense that the regge limit result is very sensitive to the manipulation of ultra-violet and infra-red cut-offs, as we have described.

In previous papers we have found that, for bound-state amplitudes in QCD, the occurrence of anomalies in multi-reggeon vertices (involving anomalous gluons) leads to an analogous sensitivity to infra-red and ultra-violet transverse momentum cut-offs. We have argued that an ultra-violet cut-off should be kept until after physical scattering amplitudes have been derived via an analysis of infra-red divergences. We anticipated that, without an initial cut-off, the ultra-violet anomaly effects would produce non-unitary power enhancement of the energy behavior of bound-state amplitudes. However, as we noted in the Introduction, accessing the anomalies in hadron amplitudes is very complicated and, therefore, it is much more difficult to appreciate their significance. In the electroweak amplitudes we have studied in this paper the anomaly appears immediately, because of the presence of elementary left-handed couplings. As a result the choice between bad, large transverse momentum based, high-energy behavior and infra-red anomaly domination producing “non-perturbative” dynamics, is also immediately clear.

Potential non-unitary properties of electroweak high-energy scattering amplitudes may not be of great concern if, as is currently believed by many physicists, the gravitational interaction intervenes long before the relevant energies are reached. From this perspective, our study of electroweak amplitudes can be viewed as simply a technical exercise in which left-handed vector mesons are used to study how, with the

cut-off manipulation we have described, the formation of QCD bound states, including confinement and chiral symmetry breaking, can take place via regge limit infra-red anomaly effects. Nevertheless, it seems hard to avoid the conclusion that if confinement and chiral symmetry breaking do not take place in this manner, then (assuming that it does not cancel) the power enhancement of quark-antiquark exchange by the ultra-violet anomaly will dominate any electroweak symmetry breaking mechanism that is perturbatively based.

Our point of view is that the unitarity of the electroweak part of the Standard Model is a deep constraint. Indeed, it could be that obtaining consistent high-energy scattering amplitudes for massive vector mesons, with left-handed couplings to quarks, may actually require QCD confinement and chiral symmetry breaking to take place via the anomaly, and may even, perhaps, require that the chiral symmetry breaking (of higher color quarks) is responsible for electroweak symmetry breaking.

We were led to the present investigation as an outcome of our study of the QCD pomeron. For a long period of time we understood the crucial role of the anomaly in producing unitary high-energy amplitudes within QCD, but were unable to find a simple starting point from which to begin construction of such amplitudes. Then, in our most recent paper[8], we showed that wee gluon properties of the pion, obtained from the anomaly, provide such a starting-point, at least in part. At the same time we realized that such properties should appear if the pion is extracted from the wee parton structure of an electroweak vector meson. This led us to the, a priori much simpler, problem of how an exchanged pion appears within the scattering of vector mesons. We now believe that the results of this paper will lead to an understanding of the pion which will, eventually, provide a simple starting point for the construction of QCD high-energy amplitudes.

Acknowledgement

I am grateful to Jochen Bartels for useful criticism of a preliminary version of this paper. I am also grateful to Bill Bardeen for valuable discussion of electroweak Ward identity cancelations.

Appendix A. Complex Notation for Transverse γ - Matrices

To discuss high-energy vector meson scattering amplitudes involving (massless) fermion exchange, it is convenient to use a complex number notation[16] for both transverse momenta and γ matrices. In this formalism, the consequences of chirality conservation and a left-handed gauge interaction are particularly apparent.

In addition to using conventional light-cone momenta $k_{\pm} = (k_0 \pm k_1)/\sqrt{2}$, we write

$$\hat{k} = k_2 + i k_3, \quad \hat{k}^* = k_2 - i k_3 \quad (A.1)$$

to describe transverse momenta. We then have

$$k_{\perp}^2 = \hat{k} \hat{k}^* \quad (A.2)$$

and

$$2k_{\perp} \cdot q_{\perp} = \hat{k} \hat{q}^* + \hat{k}^* \hat{q} \quad (A.3)$$

We can also write

$$\begin{aligned} \hat{k} \hat{q}^* &= (\hat{k}^* \hat{q})^* = k_2 q_2 + k_3 q_3 + i(k_2 q_3 - k_3 q_2) \\ &= k_{\perp} \cdot q_{\perp} + i k_{\perp} \times q_{\perp} \end{aligned} \quad (A.4)$$

where

$$k_{\perp} \times q_{\perp} = |k_{\perp}| |q_{\perp}| \sin \theta \quad (A.5)$$

with θ the angle between the two vectors.

To describe transverse γ - matrices, we similarly write

$$\hat{\gamma} = (\gamma_2 + i \gamma_3)/\sqrt{2}, \quad \hat{\gamma}^* = (\gamma_2 - i \gamma_3)/\sqrt{2} \quad (A.6)$$

We then have

$$(\hat{\gamma})^2 = (\hat{\gamma}^*)^2 = 0, \quad \hat{\gamma} \hat{\gamma}^* + \hat{\gamma}^* \hat{\gamma} = 2 \quad (A.7)$$

and we can write

$$2\hat{k}_{\perp} = \hat{k} \hat{\gamma}^* + \hat{k}^* \hat{\gamma} \quad (A.8)$$

In the regge limit the transverse part of an exchanged fermion propagator dominates, i.e. for a massless fermion

$$\frac{\hat{k}}{k^2} \rightarrow \frac{1}{2} \left(\frac{\hat{\gamma}^*}{\hat{k}^*} + \frac{\hat{\gamma}}{\hat{k}} \right) \quad (A.9)$$

where the two terms represent the two different chiralities. For example, the transverse momentum integration of a quark-antiquark state with transverse momentum q_\perp and equal chiralities (opposite sign helicities) takes the form

$$\int d^2\hat{k}_1 d^2\hat{k}_2 \delta^2(\hat{q} - \hat{k}_1 - \hat{k}_2) \left(\frac{\hat{\gamma}}{\hat{k}_1} \otimes \frac{\hat{\gamma}^*}{\hat{k}_2^*} + \frac{\hat{\gamma}^*}{\hat{k}_1^*} \otimes \frac{\hat{\gamma}}{\hat{k}_2} \right) \quad (A.10)$$

where the \otimes sign indicates that the two γ -matrices are separately associated with the two fermion lines. The contribution of a two fermion state with opposite chiralities is clearly analogous. However, the distinct combinations of same sign and opposite sign chiralities are exchanged and interact separately[16, 11]. As we elaborate on briefly in Appendix B, the very different properties of the interaction of same sign and opposite sign chirality exchanges is of fundamental importance.

If we also define

$$\hat{\Pi}_+ = -\frac{1}{2}\hat{\gamma}\hat{\gamma}^*, \quad \hat{\Pi}_- = -\frac{1}{2}\hat{\gamma}^*\hat{\gamma}, \quad \Pi_+ = \frac{1}{2}\gamma_-\gamma_+, \quad \Pi_- = \frac{1}{2}\gamma_+\gamma_- \quad (A.11)$$

then we can write

$$\gamma_5 = (\Pi_+ - \Pi_-)(\hat{\Pi}_+ - \hat{\Pi}_-) \quad (A.12)$$

Spinors in the subspaces $\Pi_-\hat{\Pi}_+$ and $\Pi_-\hat{\Pi}_-$ (or $\Pi_+\hat{\Pi}_+$ and $\Pi_+\hat{\Pi}_-$) carry opposite chirality, as is evident from the following relations

$$\begin{aligned} \gamma_-\hat{\gamma}[1 - \gamma_5]\hat{\gamma}^* &= \gamma_-[1 + \gamma_5]\hat{\gamma}\hat{\gamma}^* = \gamma_-[1 - \Pi_-\hat{\Pi}_+]\hat{\gamma}\hat{\gamma}^* \\ &= \gamma_-(1 + \frac{1}{2}\hat{\gamma}\hat{\gamma}^*)\hat{\gamma}\hat{\gamma}^* = 2\gamma_-\hat{\gamma}\hat{\gamma}^* \end{aligned} \quad (A.13)$$

$$\begin{aligned} \gamma_-\hat{\gamma}^*[1 - \gamma_5]\hat{\gamma} &= \gamma_-[1 + \gamma_5]\hat{\gamma}^*\hat{\gamma} = \gamma_-[1 + \Pi_-\hat{\Pi}_-]\hat{\gamma}^*\hat{\gamma} \\ &= \gamma_-(1 - \frac{1}{2}\hat{\gamma}^*\hat{\gamma})\hat{\gamma}^*\hat{\gamma} = 0 \end{aligned}$$

Similarly, we can show that

$$\gamma_+\hat{\gamma}^*(1 - \gamma_5)\hat{\gamma} = 0, \quad \gamma_+\hat{\gamma}^*(1 - \gamma_5)\hat{\gamma} = 2\gamma_+\hat{\gamma}^*\hat{\gamma} \quad (A.14)$$

$$\gamma_-\hat{\gamma}(1 + \gamma_5)\hat{\gamma}^* = 0, \quad \gamma_-\hat{\gamma}^*(1 + \gamma_5)\hat{\gamma} = 2\gamma_-\hat{\gamma}^*\hat{\gamma} \quad (A.15)$$

$$\gamma_+\hat{\gamma}^*(1 + \gamma_5)\hat{\gamma} = 0, \quad \gamma_+\hat{\gamma}(1 + \gamma_5)\hat{\gamma}^* = 2\gamma_+\hat{\gamma}\hat{\gamma}^* \quad (A.16)$$

For a vector particle, with momentum along the 1-axis, the polarization vectors for states with helicity $\lambda = \pm 1$ are

$$\begin{aligned}\epsilon^\mu(\lambda = +1) &= -\frac{1}{\sqrt{2}}(0, 0, 1, i) \\ \epsilon^\mu(\lambda = -1) &= \frac{1}{\sqrt{2}}(0, 0, 1, -i)\end{aligned}\quad (A.17)$$

A vector boson with helicity $\lambda = -1$ can make a transition to a left-handed intermediate state quark via the emission of an antiquark. To calculate the scattering of a vector boson with helicity $\lambda = -1$ we introduce an initial coupling of $\bar{\psi}\gamma^*(1 - \gamma_5)\psi$ and a final state coupling of $\bar{\psi}\gamma(1 - \gamma_5)\psi$. Utilising the above relations we find that, as illustrated in Fig. A1, there is only one non-zero coupling to potential quark-antiquark transverse momentum states that could be exchanged.

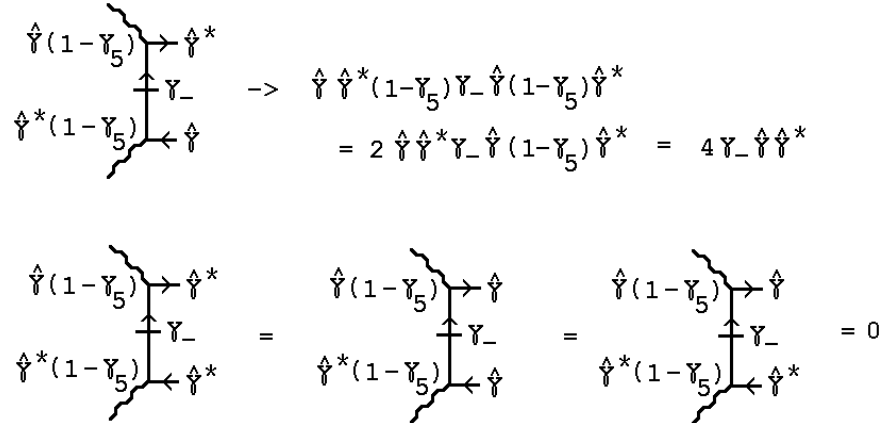


Fig. A1 Couplings to Quark-Antiquark Transverse Momentum States

As a consequence, if we consider the scattering of opposite helicity states there is only one possible lowest-order diagram, which is that shown in Fig. A2(a).

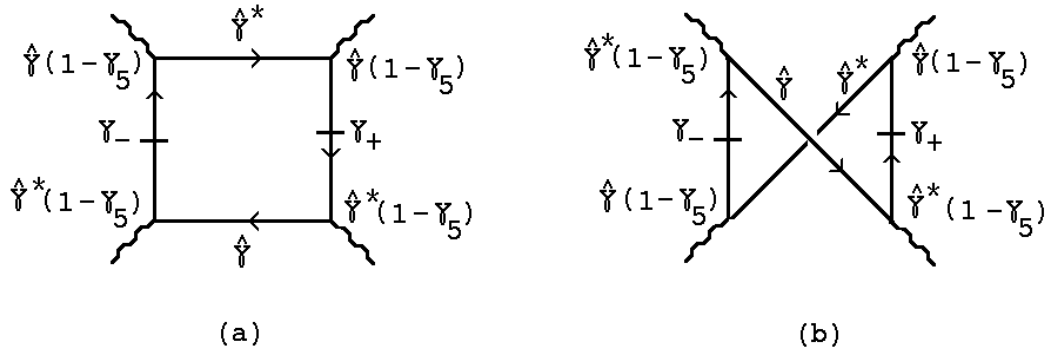


Fig. A2 Lowest-Order Diagrams

The initial $\hat{\gamma}^*(1 - \gamma_5)$ vertex on the right-hand side of Fig. A1(a) represents the coupling of a vector boson with the same polarization, but opposite helicity (since it has opposite momentum along the 1-axis) to that of the left-hand side vector boson.

A simple way to see that the diagram of Fig. 1(a) contributes to opposite helicity scattering is to note that, because of the direction of the quark arrow, the intermediate state consists of a left-handed quark, which must be produced by a negative helicity vector boson, and a right-handed antiquark, which must be produced by a positive helicity vector boson. The direction of the arrow is fixed by choosing the left-hand vector meson to be the one with negative helicity. The diagram of Fig. 1(a) contributes to the A_{-+} helicity amplitude while the diagram with the arrow reversed contributes to the A_{+-} helicity amplitude. By similar reasoning, the diagram of Fig. 2 contributes to the A_{-+} helicity amplitude.

The diagram shown in Fig. A2(b) is the only possibility for the scattering of states with equal, negative, helicities. In the cross-channel, in which the incoming and outgoing, right hand, vector mesons are interchanged, the diagram untwists to become the diagram of Fig. A1(a). Fig. A2(b) contributes to the A_{--} helicity amplitude, while the corresponding diagram with the quark arrow reversed contributes to the A_{++} helicity amplitude. For the amplitudes with π^0 quantum numbers in the t - channel, that we discuss in this paper, it follows from *CPT* invariance that

$$A_{++} = A_{--} \quad \text{and} \quad A_{-+} = A_{+-} \quad (A.18)$$

Note that, in all diagrams, only same sign chirality states are exchanged.

Appendix B. Review of Leading and Non-Leading Logs

As far as we know, the diagrams we discuss in this paper have not been discussed in detail in the literature. However, if we were to make the (wrong) assumption that the left-handed coupling does not affect the extraction of high-energy logarithms, or (more simply) if we impose a transverse momentum cut-off, there are a number of well-known results that would carry over, almost directly, into our problem. Just to put the discussion of this paper in context, we give here a very brief, non-technical, overview[11] of these results.

All the results concern the extraction of leading and non-leading logarithms. If we organize the quark-antiquark exchange diagrams into distinct series, as illustrated in Fig. B1, depending on the power of α_s (the QCD coupling) involved, then typical diagrams giving such logarithms are

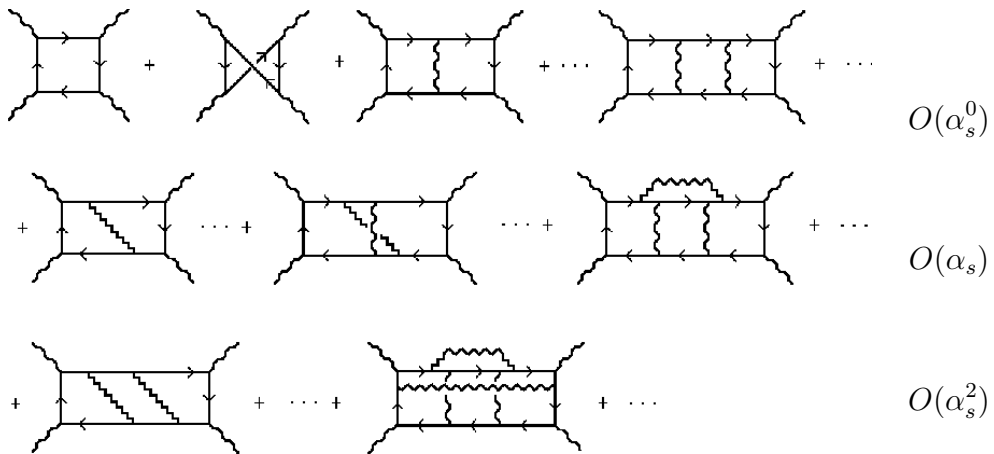


Fig. B1 Quark-Antiquark Exchange Diagrams Organized According to Powers of α_s .

The first series contains purely electroweak diagrams that have a logarithmic expansion in α_w (the “electroweak” coupling). The second series contains $O(\alpha_s)$ corrections to the first series, the third series contains $O(\alpha_s^2)$ corrections to the first series, etc.

All diagrams of the form shown in Fig. B1 would be expected to give high-energy amplitudes of the form

$$A(S, 0) \underset{S \rightarrow \infty}{\sim} \sum_{n,m,r} a_{n,m,r} \alpha_w^n \alpha_s^m [\ln S]^r \quad (B.1)$$

To make our discussion straightforward we can suppose that we, initially, introduce a transverse momentum cut-off so that we can ignore ultra-violet transverse momentum

divergences - including both the anomaly power divergences that we discuss in this paper, and the logarithmic divergences that we discuss below. As a result, all the coefficients a_{nmr} can be represented as (sums of) transverse momentum diagrams of the form illustrated in Fig. B2.

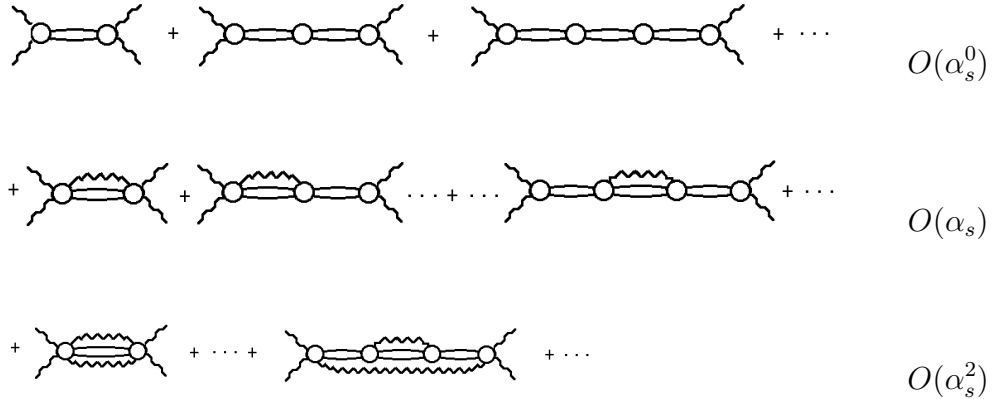


Fig. B2 Transverse Momentum Diagrams Originating from the Diagrams of Fig. B2

With the transverse momentum cut-off in place, the first two diagrams in Fig. B1 give a leading log amplitude which contains the first diagram in Fig. B2 multiplied by $\ln S$ and a next-to-leading log amplitude which contains the same transverse momentum diagram but with no factor of $\ln S$. The third diagram in Fig. B1 gives a leading log amplitude which contains the second diagram in Fig. B2 multiplied by $\ln^2 S$ and a next-to-leading log amplitude which contains the first diagram in Fig. B2 multiplied by $\ln S$ and so on. In general, the external couplings and the internal vertices in the transverse momentum diagrams acquire more and more structure (involving loop integrals) as first leading logs, then next-to-leading logs, next-to-next-to-leading logs, etc., are included in the sum (B.1).

The diagram of Fig. 2, appearing in Section 3, is the last diagram shown explicitly in the second row of Fig. B1. It is first-order in α_s and, conventionally, as noted in Section 3, we would expect that it's leading-log contribution would contain the last $O(\alpha_s)$ transverse momentum diagram shown explicitly in Fig. B2 - with simple vertices. This diagram being obtained by placing all vertical lines on-shell, as in Fig. 5 using longitudinal momentum integrations. At the next-to-leading log level the second $O(\alpha_s)$ transverse momentum diagram should be generated and the first $O(\alpha_s)$ transverse momentum diagram, which is the diagram that appears in Fig. 1, should be generated by Fig. 2 at the next-to-next-to-leading log level.

The transverse momentum diagram of Fig. 27 is the first $O(\alpha_s^2)$ diagram appearing in Fig. B2 and would be generated, at leading log, by the first $O(\alpha_s^2)$ diagram

in Fig. B2. The diagram of Fig. 20 is the second $O(\alpha_s^2)$ diagram appearing explicitly in Fig. B1. The anticipated leading log result for this diagram would be $\ln^5 S$ multiplied by the second $O(\alpha_s^2)$ transverse momentum diagram appearing explicitly in Fig. B2 and the first $O(\alpha_s^2)$ diagram in Fig. B2 would be generated at the next-to-next-to-leading log level, i.e. multiplied by a factor of $\ln^3 S$.

In the leading and non-leading-log studies of pure vector gauge theories[5] there is no problem with ultra-violet divergences, either in transverse momentum, or more generally. Only the normal (ultra-violet) divergences associated with renormalization have appeared in the non-leading-log vertices. The Ward identities of the gauge theory produce cancelations that lead always to convergent transverse momentum integrals, with the accompanying logarithms just those predicted by regge theory. (Even though, as is very well known by now, individual feynman diagrams produce transverse momentum divergences that, at first sight, produce additional logarithms beyond those anticipated by regge theory.) Equivalently, the complete sum of logarithms and transverse momentum diagrams can be rearranged[2] into sub-series represented by reggeon diagrams.

When fermions are involved there is, as we already noted in Section 3, the extra subtlety of the logarithmic divergence of fermion transverse momentum integrals[11, 16]. Therefore, if the transverse momentum cut-off is removed, extra powers of $\ln S$ will be generated and the series (B.1) must be rearranged appropriately. However, fermion reggeization is not affected by the divergences (since the relevant transverse momentum integrals involve combinations of fermions and gluons). Consequently, as we noted in Section 3, when the transverse momentum diagrams are organized into reggeon diagrams, the presence of the reggeon propagator reduces the divergence from log to log[log] form. Also, the reggeon kernel for opposite sign helicities gives convergent integrals. (As we noted in the previous Appendix, the distinct combinations of opposite and same sign helicities are exchanged and interact separately.) Only the kernel for opposite sign helicities (same sign chiralities) produces logarithmic divergences at large transverse momentum.

In the diagrams discussed in this paper, the quark-antiquark states we consider are same sign chirality states. However, the anomaly enhancement overwhelms the logarithmic divergence that would otherwise result. We believe this is important, physically. If we start with a transverse momentum cut-off both the anomaly power divergence and the logarithmic divergence will be absent. When the confinement and chiral symmetry breaking described in Section 5 is implemented via the extraction of infra-red divergences, it may be (and the results of [8] directly suggest this) that only (transverse momentum) convergent same sign helicity exchanges are involved in forming bound states. Since “double logs” are, a priori, in conflict with regge theory, this is probably necessary for the bound states to be described by regge theory.

Appendix C. The Anomaly and Vector Ward Identities

To understand the special nature of Ward identities in the presence of the anomaly, it is helpful to recall some well-known properties of the one loop contribution, shown in Fig. C1, of massless fermions to an axial-vector/two-vector three current vertex $T_{\mu\alpha\beta}(k_1, k_2)$.

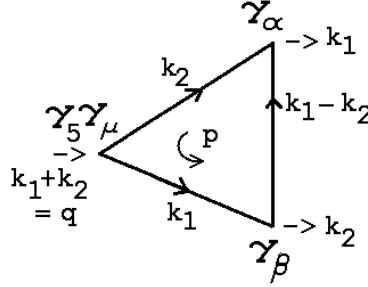


Fig. C1 The Fermion Loop Contribution to $T_{\mu\alpha\beta}(k_1, k_2)$

After decomposition into invariant amplitudes

$$\begin{aligned} T_{\mu\alpha\beta}(k_1, k_2) = & A_1 \epsilon_{\sigma\alpha\beta\mu} k_1^\sigma + A_2 \epsilon_{\sigma\alpha\beta\mu} k_2^\sigma + A_3 \epsilon_{\delta\sigma\alpha\mu} k_{1\beta} k_1^\delta k_2^\sigma \\ & + A_4 \epsilon_{\delta\sigma\alpha\mu} k_{2\beta} k_1^\delta k_2^\sigma + A_5 \epsilon_{\delta\sigma\beta\mu} k_{1\alpha} k_1^\delta k_2^\sigma + A_6 \epsilon_{\delta\sigma\beta\mu} k_{2\alpha} k_1^\delta k_2^\sigma \end{aligned} \quad (C.1)$$

the vector Ward identities

$$k_1^\alpha \Gamma_{\mu\alpha\beta} = 0, \quad k_2^\beta \Gamma_{\mu\alpha\beta} = 0 \quad (C.2)$$

require

$$A_2 = k_1^2 A_5 + k_1 \cdot k_2 A_6 \quad (C.3)$$

$$A_1 = k_2^2 A_4 + k_1 \cdot k_2 A_3 \quad (C.4)$$

The large momentum region (with appropriate regularization) gives an “anomaly” contribution to A_1 and A_2 of the form

$$T_{\mu\alpha\beta}(k_1, k_2) = \frac{1}{4\pi^2} \epsilon_{\sigma\alpha\beta\mu} k_1^\sigma + \frac{1}{4\pi^2} \epsilon_{\sigma\alpha\beta\mu} k_2^\sigma + \dots \quad (C.5)$$

leading to the well-known “anomalous” divergence equation

$$(k_1 + k_2)^\mu T_{\mu\alpha\beta} = \frac{1}{2\pi^2} \epsilon_{\delta\sigma\alpha\beta} k_1^\delta k_2^\sigma \quad (C.6)$$

For the vector Ward identities to hold in the presence of (C.5), there must be related, infra-red singular, contributions to the other A_i . For example, when $k_1^2 = 0$, (C.3) becomes

$$A_2 = k_1 \cdot k_2 A_6 = \frac{q^2 - k_2^2}{2} A_6 \quad (C.7)$$

implying that there must be a pole in A_6 , arising from the region of small internal momentum. In appropriate circumstances, this pole can be interpreted as a Goldstone boson pole, signaling chiral symmetry breaking.

If we consider $k_1 \rightarrow 0$, and assume that all the A_i are sufficiently non-singular, then (C.1) gives

$$\begin{aligned} T_{\mu\alpha\beta}(k_1, k_2) &\rightarrow A_2 \epsilon_{\sigma\alpha\beta\mu} k_2^\sigma \\ k_1 \rightarrow 0 & \end{aligned} \quad (C.8)$$

which, if we keep only the ultra-violet anomaly term (C.5), gives

$$T_{\mu\alpha\beta}(k_1, k_2) \underset{k_1 \rightarrow 0}{\rightarrow} \frac{1}{4\pi^2} \epsilon_{\sigma\alpha\beta\mu} k_2^\sigma \neq 0 \quad (C.9)$$

Alternatively, if we use (C.3), together with (C.8), we obtain

$$T_{\mu\alpha\beta}(k_1, k_2) \underset{k_1 \rightarrow 0}{\rightarrow} (k_1^2 A_5 + k_1 \cdot k_2 A_6) \epsilon_{\sigma\alpha\beta\mu} k_2^\sigma \rightarrow 0 \quad (C.10)$$

For consistency, again, there must be infra-red singular contributions to $T_{\mu\alpha\beta}(k_1, k_2)$ that cancel the ultra-violet anomaly contribution (C.5) and produce the “Ward identity zero” (C.10).

From our point of view, therefore, the presence of the ultra-violet anomaly (C.5) has two consequences. The first is the anomalous Ward identity (C.6). The second is that the vector Ward identities require a cancelation between separate contributions (with different kinematic structure) from large and small internal momentum regions. As a consequence, if an explicit ultra-violet cut-off is introduced, (C.5) will be modified and the vector Ward identities will no longer hold. The contribution, to the vector current divergence, of the pole term in A_6 will survive, however, since it is generated in the infra-red region[8].

Appendix D. Electroweak Ward Identity Cancelations

In this Appendix we consider whether Ward identity cancelations can remove the longitudinal polarization contributions of vector mesons that produce the anomaly enhanced high-energy behavior in the diagrams we have discussed. As described in sub-section 3.13, we are interested in Ward identity implications when we add all the diagrams that effectively replace the tree diagram that forms the lower part of Fig. 1 by another tree diagram. As in Section 3, it will be sufficient for our purposes to consider only the diagrams of an abelian theory.

We focus on the same region of phase space as in Section 3, which will be the basis for all approximations we make. If we ignore $(1 - \gamma_5)$ factors (which are irrelevant for the present discussion), the lower part of Fig. 1 gives the amplitude shown in Fig. D1

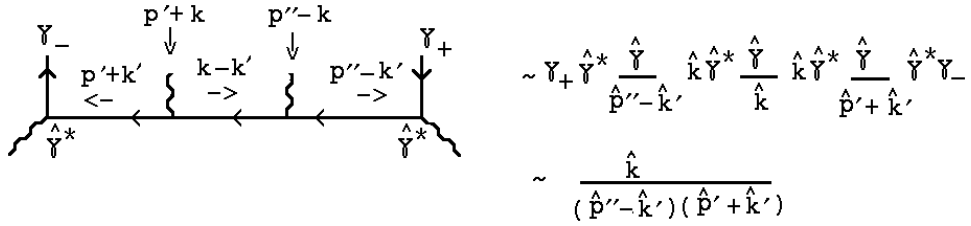


Fig. D1 The Tree Diagram Obtained From Fig. 1.

We consider, first, the addition of tree diagrams in which the internal left-side vector boson line is attached at all possible points. We begin with the diagrams obtained by moving this line to the right.

The subdiagram forming the left part of Fig. D1 can be split into two pieces as illustrated in Fig. D2.

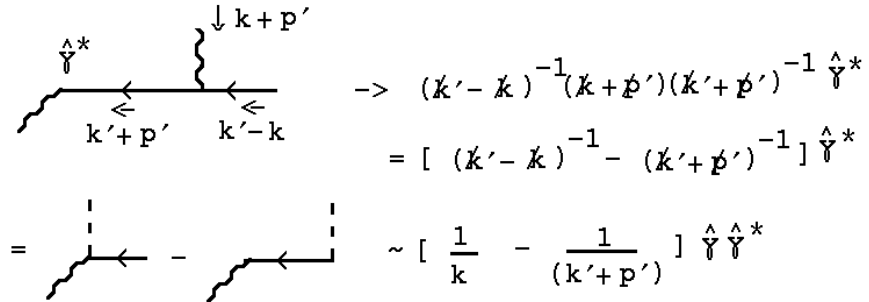


Fig. D2 Splitting Fig. D1

where the dashed line indicates that additional momentum flows in to a vertex without changing the algebraic structure. It is the Ward identity cancelation for the second

piece of Fig. D2 that involves moving the vector boson line to the right. Note, first, that if we combine this term with the right-side of the full diagram we obtain the amplitude shown in Fig. D3

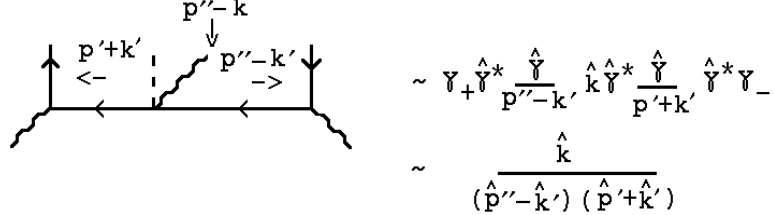


Fig. D3 The Amplitude Obtained From the Second Term of Fig. D2

and so the relevant piece of Fig. D1 is retained.

The first tree diagram obtained by moving the left side internal vector meson to the right is the second diagram appearing in Fig. 16, which is the lower part of the feynman diagram appearing in Fig. 17. We consider the right part of this tree diagram and divide it into two pieces as in Fig. D4.

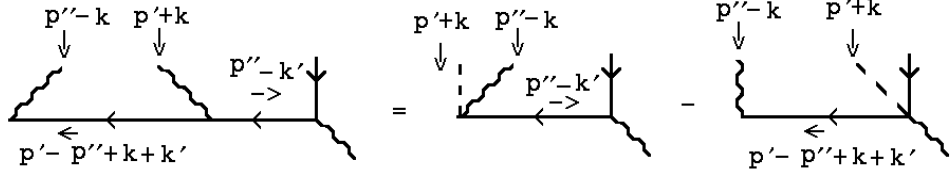


Fig. D4 Splitting of Another Tree Diagram

The first piece gives an amplitude that directly cancels the amplitude of Fig. D3. Therefore, it would appear that the amplitude involved in the anomaly enhancement is immediately eliminated. However, there are further cancellations that remain to be discussed.

The second piece of Fig. D4 has to be combined with the contribution of the tree diagram shown in Fig. D5.

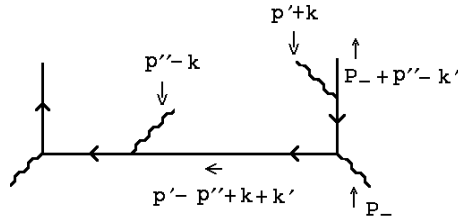


Fig. D5 Another Tree Diagram

Making the usual separation (into two pieces) of the right side of the tree diagram appearing in Fig. D5 and removing the piece that cancels with the second piece of Fig. D4 leaves the piece shown in Fig. D6.

$$\begin{aligned}
 & \text{Diagram:} \\
 & \text{Vertical line: } p''-k \downarrow \\
 & \text{Horizontal line: } p_- \uparrow \quad \text{bracket below: } < p' - p'' + k + k' \\
 & \text{Dashed line: } p'+k \downarrow \\
 & \text{Equation:} \\
 & = \gamma_+(\not{p}_- + \not{p}'' - \not{k}') (\not{p}_- + \not{p}'' - \not{k}' - \not{p}' - \not{k})^{-1} \hat{\gamma}^* (\not{p}' - \not{p}'' + \not{k} + \not{k}')^{-1} (\not{p}'' - \not{k}) \\
 & \sim \gamma_+ \frac{\hat{\gamma}}{\not{p}'' - \not{k}'} \gamma_- p'_+ (p'_+ p_-)^{-1} \hat{\gamma}^* \gamma_- p'_+ (p'_+ p''_+)^{-1} \gamma_+ p''_+ \\
 & \sim \frac{(\hat{\not{p}''} - \hat{\not{k}'})}{p_-}
 \end{aligned}$$

Fig. D6 Part of the Tree Diagram Appearing in Fig. D5

This piece would be zero if the vertical antiquark were exactly, and not just approximately, on-shell.

Since the amplitude of Fig. D6 goes to zero as $P_- \rightarrow \infty$, with all internal momenta fixed, it is, superficially, a non-leading asymptotic contribution. However, it has worse large transverse momentum behavior than the original amplitude of Fig. D2. In effect, we have replaced a leading asymptotic contribution that has manageable internal momentum behavior with a superficially non-leading contribution with bad internal momentum behavior. At this point, this substitution does not actually lead to any important effects, although this will not be the case for an analogous substitution that we make later. We obtain the maximal contribution from the amplitude of Fig. D6 if we use the mass-shell condition $P_- k'_- \sim (p''_+ - k'_+)^2$ and combine the resulting amplitude with the second term in Fig. D2. This gives

$$\left(\frac{k'_-^2}{k_-} \right) \frac{1}{(\hat{p}' + \hat{k}') (p''_+ - k'_+)} \quad (D.1)$$

This amplitude does not have the growth at large k'_+ that the amplitude of Fig. D1 has and so can be neglected.

We now consider the contribution of the first term in Fig. D2. This has to be combined with tree diagrams obtained by moving the left side internal vector meson line to the left. There is only one such diagram, which is shown in Fig. D7.

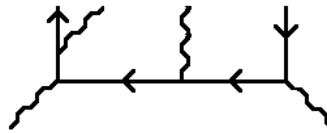


Fig. D7 Another Tree Diagram

Normally this contribution to the high-energy limit would be ignored because an off-shell propagator carries the large P_+ momentum. However, if we split this diagram into two pieces as in Fig. D8,

$$\begin{aligned}
 & \text{Diagram 1:} \\
 & \text{Diagram 2:} \\
 & \text{Diagram 3:}
 \end{aligned}$$

Fig. D8 Splitting The Diagram of Fig. D7

the first piece cancels with the first piece of Fig. D2.

If the vertical quark line were on shell so that the full numerator, and not just the asymptotic γ_- piece, were present, the second piece of Fig. D8 would be zero. In fact, if we use the mass-shell condition $P_+ k'_- \sim (p'_\perp + k'_\perp)^2$ we obtain

$$\frac{(\hat{p}' + \hat{k}')^*)}{P_+ k_-} \sim \frac{k'_-}{k_-} \frac{(\hat{p}' + \hat{k}')^*)}{(p'_\perp + k'_\perp)^2} = \frac{k'_-}{k_-} \frac{1}{(\hat{p}' + \hat{k}')} \quad (D.2)$$

Since both k'_- and k_- are finite in the momentum region we are considering, (D.2) is of the same form as the second term in Fig. D2. In this case, therefore, a superficially non-leading asymptotic contribution, with bad large transverse momentum behavior, gives a contribution that can not be neglected.

We now consider the additional tree diagrams that would be involved in a Ward identity for the right side internal vector meson line. From the above discussion it follows that, after we have added all such diagrams and carried out the analogous cancellations to those above, there will be one surviving contribution that will give an amplitude of the form of Fig. D1. This will come from the tree diagram shown in Fig. D9.

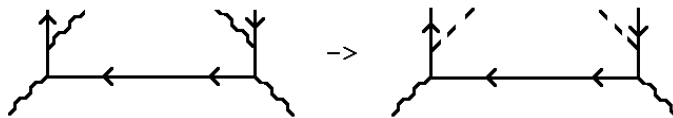


Fig. D9 The Tree Diagram Giving the Surviving Amplitude

The piece of this diagram that we have picked out would vanish if both the quark and antiquark vertical lines were on-shell. From Fig. D8 and (D.2) it is clear that this piece gives a “superficially non-leading” amplitude of the form

$$\frac{(\hat{p}' + \hat{k}')^*}{P_+ k_-} \hat{k} \frac{(\hat{p}'' - \hat{k}')^*}{P_- k_+} \quad (D.3)$$

which, after we use the mass-shell conditions for P_+ and P_- , gives the amplitude

$$\left(\frac{k'_+ k'_-}{k_+ k_-} \right) \frac{\hat{k}}{(\hat{p}' + \hat{k}')(\hat{p}'' - \hat{k}')} \quad (D.4)$$

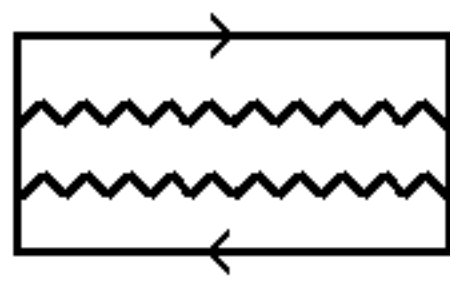
Since both $k'_+ k'_-$ and $k_+ k_-$ are finite, this is, indeed, an amplitude of the form of Fig. D1.

We conclude that the large transverse momentum behavior of the amplitude in Fig. 3, which combines with the loop amplitude in the top half of Fig. 1 to give the anomaly, does not cancel after the imposition of Ward identities. In this respect, therefore, nothing is gained by implementing the Ward identity cancelations. However, the lack of cancellation is entirely due to the asymptotic on-shell nature of the quark and antiquark lines. This raises a general issue of principle. Including the remaining amplitude that would put these lines exactly on-shell would apparently cancel the behavior (D.4). Yet this amplitude would normally be neglected as contributing only to non-leading high-energy behavior. It can contribute to the leading behavior only if there are large transverse momentum divergences. In fact, as we have emphasized, to carry out the Ward identity cancelations we have actually included several diagrams that would normally be considered non-leading.

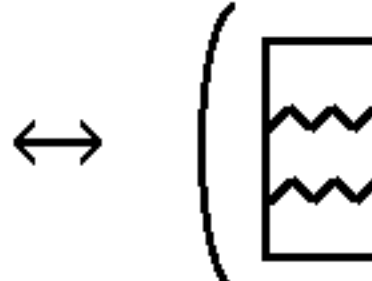
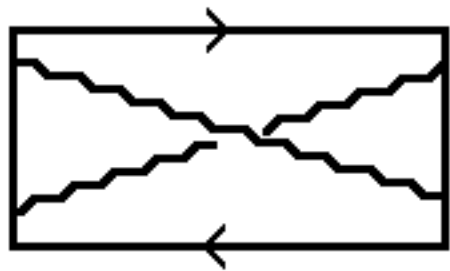
The normal procedure is to effectively assume in advance (and then justify a *posteriori*) that transverse momenta will be sufficiently cut-off after the summation over all diagrams. The leading parts of diagrams can then be safely extracted without worrying about transverse momentum divergences. The occurrence of the anomaly enhancement phenomenon in the diagrams that we have discussed could imply that in many other diagrams large transverse momenta are also sufficiently important that the normal methods are inadequate. If this is the case, then it is likely that the general transverse momentum diagram formalism will fail. Since there would then be no reggeon diagram formalism, *t*-channel unitarity is also likely to fail. The conclusion, which is really the main conclusion of this paper, is that to use the transverse momentum diagram formalism (and therefore to ensure *t*-channel unitarity) it is essential to initially employ a transverse momentum cut-off.

References

- [1] V. S. Fadin, E. A. Kuraev and L. N. Lipatov, *Sov. Phys. JETP* **45**, 199 (1977).
- [2] J. B. Bronzan and R. L. Sugar, *Phys. Rev.* **D17**, 585 (1978), this paper organizes into reggeon diagrams the results from H. Cheng and C. Y. Lo, *Phys. Rev.* **D13**, 1131 (1976), **D15**, 2959 (1977).
- [3] V. S. Fadin and V. E. Sherman, Sov. Phys. JETP **45**, 861 (1978).
- [4] V. S. Fadin and L. N. Lipatov, *Nucl. Phys.* **B406**, 259 (1993).
- [5] V. S. Fadin and L. N. Lipatov, *Nucl. Phys.* **B477**, 767 (1996) and further references therein.
- [6] J. Bartels, *Z. Phys.* **C60**, 471 (1993) and further references therein.
- [7] A. R. White, *Int. J. Mod. Phys.* **A8**, 4755 (1993).
- [8] A. R. White, *Phys. Rev.* **D66**, 056007 (2002).
- [9] A. R. White, *Phys. Rev.* **D66**, 045009 (2002).
- [10] A. R. White, *Phys. Rev.* **D29**, 1435 (1984).
- [11] For a detailed review and further references, see R. Kirschner, *Nucl. Phys. Proc. Suppl.* **51C**, 118 (1996).
- [12] G. 't Hooft, *Nucl. Phys.* **B33**, 173 (1971).
- [13] S. l. Adler and W. B. Bardeen, *Phys. Rev.* **182** 1517-1536 (1969).
- [14] A. R. White, *Phys. Rev.* **D58**, 074008 (1998).
- [15] A. A. Migdal, A. M. Polyakov and K. A. Ter-Martirosyan, *Zh. Eksp. Teor. Fiz.* **67**, 84 (1974); H. D. I. Abarbanel and J. B. Bronzan, *Phys. Rev.* **D9**, 2397 (1974).
- [16] R. Kirschner, L. Mankiewicz, A. Schafer and L. Szymanowski, *Z. Phys.* **C74**, 501 (1997).



+



$$+ \rightarrow \begin{array}{c} \nearrow \\ \searrow \end{array} = \{0\}, \{8\} \quad \begin{array}{c} \text{wavy line} \end{array} =$$

$$- \rightarrow \begin{array}{c} \nearrow \\ \searrow \end{array} = \{8\} \quad \begin{array}{c} \text{wavy line} \end{array} =$$